AGU PUBLICATIONS

Geochemistry, Geophysics, Geosystems

RESEARCH ARTICLE
10.1002/2015GC005748

Key Points:
- Modeling of Martian aqueous processes leading to Li isotope fractionation
- Li isotopic data relevant to understand early Mars environmental conditions
- Evaporation, sublimation, and freezing processes included in the models

Supporting Information:
- Supporting Information S1

Correspondence to:
A. G. Fairén,
agfairen@cab.inta-csic.es

Citation:
Fairén, A. G., E. Losa-Adams, C. Gil-Lozan, L. Gago-Duport, E. R. Uceda, S. W. Squyres, J. A. P. Rodríguez, A. F. Davila, and C. P. McKay (2015), Tracking the weathering of basalts on Mars using lithium isotope fractionation models, *Geochem. Geophys. Geosyst.*, *16*, 1172–1197, doi:10.1002/2015GC005748.

Received 30 JAN 2015
Accepted 24 MAR 2015
Accepted article online 28 MAR 2015
Published online 28 APR 2015

The copyright line for this article was changed on 19 MAY 2016 after original online publication.

Tracking the weathering of basalts on Mars using lithium isotope fractionation models

Alberto G. Fairén[1,2], Elisabeth Losa-Adams[3], Carolina Gil-Lozano[3], Luis Gago-Duport[3], Esther R. Uceda[4], Steven W. Squyres[2], J. Alexis P. Rodríguez[5], Alfonso F. Davila[6], and Christopher P. McKay[5]

[1]Centro de Astrobiología, Madrid, Spain, [2]Department of Astronomy, Cornell University, Ithaca, New York, USA, [3]Departamento de Geociencias Marinas, Universidad de Vigo, Vigo, Spain, [4]Departamento de Biología Molecular, Universidad Autónoma de Madrid, Madrid, Spain, [5]Space Science and Astrobiology Division, NASA Ames Research Center, Mountain View, California, USA, [6]SETI Institute, Mountain View, California, USA

Abstract Lithium (Li), the lightest of the alkali elements, has geochemical properties that include high aqueous solubility (Li is the most fluid mobile element) and high relative abundance in basalt-forming minerals (values ranking between 0.2 and 12 ppm). Li isotopes are particularly subject to fractionation because the two stable isotopes of lithium—^{7}Li and ^{6}Li—have a large relative mass difference (~15%) that results in significant fractionation between water and solid phases. The extent of Li isotope fractionation during aqueous alteration of basalt depends on the dissolution rate of primary minerals—the source of Li—and on the precipitation kinetics, leading to formation of secondary phases. Consequently, a detailed analysis of Li isotopic ratios in both solution and secondary mineral lattices could provide clues about past Martian weathering conditions, including weathering extent, temperature, pH, supersaturation, and evaporation rate of the initial solutions in contact with basalt rocks. In this paper, we discuss ways in which Martian aqueous processes could have lead to Li isotope fractionation. We show that Li isotopic data obtained by future exploration of Mars could be relevant to highlighting different processes of Li isotopic fractionation in the past, and therefore to understanding basalt weathering and environmental conditions early in the planet's history.

1. Introduction

1.1. Lithium Isotope Geochemistry

Lithium (Li) isotope geochemistry investigations provide important information about the balance between silicate-bearing minerals in source rocks and the geochemical processes associated with the weathering of primary silicates in aqueous environments [see, e.g., *Chan et al.*, 1992; *Hathorne and James*, 2006; *Decarreau et al.*, 2012; *Ryu et al.*, 2014]. Usually Li can be found, in the range of ppm, in almost all primary minerals present in basalt because of its small ionic radius, similar to Mg [*Seitz and Woodland*, 2000; *Seitz et al.*, 2006; *Tang et al.*, 2007; *Brant et al.*, 2012].

The two stable isotopes of lithium—^{7}Li and ^{6}Li—have a large relative mass difference (~15%) that results in significant fractionation between water and solid phases, providing important information on chemical weathering processes [*Chan et al.*, 1992, 1994]. Dissolution of basalt occurs according to a congruent mechanism, which by itself does not cause an appreciable fractionation [*Wimpenny et al.*, 2010]; however, isotopic fractionation takes place as a result of ion exchange processes between water and solid phases [*Taylor and Urey*, 1938; *Huh et al.*, 1998, 2004; *Kisakurek et al.*, 2005]. Secondary minerals, in particular clays, preferentially incorporate the lighter isotope in their structural lattice, thus leaving the remaining water with a heavier isotopic signature [*Zhang et al.*, 1998; *Vigier et al.*, 2008; *Misra and Froelich*, 2012]. Significant fractionation also occurs after the formation of oxyhydroxides and hydroxides, like ferrihydrite or gibbsite. Variations in δ^{7}Li produced by aqueous alteration are appreciable only a few milimeters below the basaltic rocks' surface: rock surfaces are lighter in δ^{7}Li than the interiors, due to the preferential incorporation of ^{6}Li in clays or oxide-rich alteration products on the surface [*Pistiner and Henderson*, 2003].

Variations in the Li isotope ratios of both seawater and secondary minerals are mainly a function of the alteration degree, conducing to the formation of different amounts and types of secondary minerals, and therefore can be used as an indicator of weathering conditions and rates (the variation in seawater is due

more to differing weathering rates than to differring weathering conditions). For example, the value of δ^7Li in terrestrial seawater (δ^7Li_{sw}) is now 31‰, but it rose by 9‰ during the last 60 million years as reflected in analyses of clays and planktonic foraminifera [*Kisakurek et al*., 2005; *Hathorne and James*, 2006; *Misra and Froelich*, 2012; *Pogge von Strandmann et al*., 2013], indicating lower continental weathering and denudation rates in the past.

In global terms, δ^7Li_{sw} characterizes the weathering intensity as an interplay of two processes: the uptake of Li by secondary minerals, which leads to heavy signatures in the riverine input [*Liu et al*., 2015] and lowers Li concentration, and the amount of Li directly derived from the disolution of igneous rocks by chemical weathering with light isotopic signature. Additional processes, such as hydrothermal alteration and formation of secondary minerals in sediments via reverse weathering, may be important in modifying the Li isotope signatures at local scales, as observed in hydrothermal vents [*Decitre et al*., 2004] and in estuarine environments [*Pogge von Strandmann et al*., 2008]. These processes might be significant in the context of hypothetical early water bodies on Mars, where the precipitation of secondary phases could have been controlled by the balance between evaporation and cooling [*Fairén et al*., 2009], through reverse weathering processes.

1.2. Lithium Isotope Geochemistry and Mars

1.2.1. Meteorite and MSL-Derived Information About Li in Mars

Most lander and rover missions to Mars have lacked a way to identify light elements such as lithium, and therefore the presence of Li on Mars has been so far just inferred from measurements of lithium isotopes in the SNC-meteorites Shergotty, Nakhla, and Zagami [e.g., *McSween et al*., 2001; *Herd et al*., 2004, 2005; *Treiman et al*., 2006; *Magna et al*., 2006; *Seitz et al*., 2006, 2007; *Möhlmann and Thomsen*, 2011; *Filiberto et al*., 2012]. As a result, extensive past work on Li isotopes in Martian meteorites has focused on how isotope fractionation patterns can yield insight into Martian igneous processes [e.g., *Beck et al*., 2004; *Seitz et al*., 2006]. Only the most recent mission to the Martian surface, the Mars Science Laboratory (MSL) *Curiosity* rover, which landed in Gale crater in August 2012 and is currently exploring the Martian surface, includes for the first time the capacity of directly detecting lithium, via its ChemCam instrument [*Wiens et al*., 2012]. Lithium contents measured by MSL in materials within Gale crater are low and variable, mainly between 5 and 10 ppm, similar to terrestrial mid-ocean ridge basalts (MORB, ~4–5 ppm) [e.g., *Chan et al*., 1992]. Maxima are up to 60–80 ppm, observed in a few rocks, and minima are <5 ppm inside drill holes [*Ollila et al*., 2013]. In general, the concentration is low in soils and sand, consistent with a vapor-transport mechanism, and higher in rocks and pebbles [*Ollila et al*., 2014]. Smectite clays, such as montmorillonite or hectorite, have been suggested as possible host minerals for the Li identified in Mars with MSL [*Ollila et al*., 2014].

1.2.2. Expected Information From In Situ Sampling of Li Isotopes

Lithium incorporation into a secondary mineral is a solvent-mediated process that can provide information about the duration, extent, and conditions of aqueous interaction between primary minerals and water. But Li isotopes could provide additional information when compared to Li abundances alone: the selective incorporation of the lighter isotope to secondary minerals, and consequently the evolution through time of the Li isotopic signature, reflects the interaction between chemical and physical weathering processes that are unequally affected by changes of pH and temperature [e.g., *Ryu et al*., 2014]. In Earth's oceans, the actual steady state for δ^7Li_{sw} physically represents the balance between the amount of Li dissolved and amount of Li trapped on the secondary mineral lattices. In the end, such a balance can be related to the ocean evolution toward a stationary pH, being that pH is the main factor influencing the equilibrium between dissolution and precipitation of silicates, according to the overall silicate-carbonate geochemical cycle. On Mars, presumably this evolution has been rather different than on Earth, subject to evaporation, sublimation and freezing, and probably never reaching a steady state for pH conditions.

1.3. Objctives of This Work

In this paper, we discuss ways in which Martian aqueous processes could lead to Li isotope fractionation and their eventual incorporation into secondary minerals. Secondary minerals are abundant on Mars, and phyllosilicate-rich outcrops have been identified in the Noachian terrains of the Martian southern highlands, which include Fe/Mg-smectites (hectorite, nontronite, and saponite), Al-smectites (montmorillonite and beidellite), vermiculite, illite, chlorite, and kaolinite [see, e.g., *Mustard et al*., 2008; *Bishop et al*., 2008; *Le Deit et al*., 2012; *Ehlmann et al*., 2013]. For a review of the geochemical and hydrological evolution of Mars

through time, relevant for the understanding of the changing environment of the planet, the reader is referred to *Chevrier et al*. [2007], *Hurowitz et al*. [2010], *Fairén et al*. [2011], and *Ehlmann et al*. [2013]. We present geochemical models intended to help understand the Li isotopic composition of basaltic rocks and secondary minerals on Mars. We describe different case studies of Li isotope fractionation, and we discuss different Li isotope fractionation pathways. We show that our models are relevant to understand the degree and extent of basalt weathering on Mars, and therefore can be useful to determine the environmental conditions on the planet in the past.

2. Methods

2.1. Modeling of the Mechanisms of Li Uptake by Secondary Minerals

Lithium is incorporated as a trace element in most primary minerals in basalts, namely, olivines, clinopyroxenes, and Ca-plagioclase feldspars, where Li abundance varies in the order of 0.2–12 ppm [see, e.g., *Chan et al*., 2002; *Teng et al*., 2008; *Wimpenny et al*., 2010; *Brant et al*., 2012]. Within this interval, there is little variation between coexisting minerals in the average Li content and their isotopic signatures. Consequently, in the absence of secondary phases, the preferential weathering of primary minerals (driven by kinetic constraints) should not generate significant differences in the Li isotope composition of the solution [*Chan and Frey*, 2003; *Burton and Vigier*, 2011]. However, in principle and based on theoretical considerations, breaking the higher energy bonds of ^{6}Li is energetically favorable, leading to a slightly lighter isotope composition in solution than in the host minerals. This effect has not been experimentally demonstrated to date, nor it has been incorporated to models dealing with Li isotope behavior on Earth. Furthermore, the experimental results from *Wimpenny et al*. [2010], based on the dissolution of forsterite and basaltic glass, indicate that both crystalline and amorphous phases dissolve congruently with respect to Li isotopes.

The particular isotopic signature of basaltic rocks can vary depending on their petrogenetic provenance. For modeling purposes, we assume an initial value of $\delta^{7}\mathrm{Li} = 5‰$ that corresponds to the average isotopic signature of unweathered MORB basalts [*Tomascak*, 2004; *Tang et al*., 2007]. This signature is similar to the majority of Martian basalts (Nakhla $\delta^{7}\mathrm{Li} = +4.99 \pm 0.47‰$; Lafayette $\delta^{7}\mathrm{Li} = +5.0 \pm 0.7‰$) derived from analyses of SNC meteorites [*Magna et al*., 2006; *Seitz et al*., 2006].

According to the above analysis, we also assume that the Li isotopes involved in each idividual mineral or amorphous phase dissolves stoichiometrically, providing the incorporation of both isotopes, ^{7}Li and ^{6}Li, to the solution in the same ratio as in the host mineral. The primary mineralogy also determines the composition of the solution and the formation of secondary minerals. At each instant of the process, the total amount of Li in solution and its isotopic signature depend on the interplay between the specific dissolution behavior of each primary mineral existing in the rock (given as a function of its individual thermodynamic and kinetic parameters, namely, supersaturation, rate constants, and reactive surface) and the crystallization kinetics of secondary minerals. The latter can act as a sink for lithium, controlling both the remaining fraction of Li in solution and the process of isotope fractionation. Isotope fractionation is mediated by the preferential incorporation of the ligher isotope ^{6}Li into some of the solid phases which are forming as secondary minerals, especially clays. Significant fractionation also occurs after the formation of oxihydroxides and hydroxides, like ferrihydrite or gibbsite. Although Li isotope fractionation into solid phases always implies a preferential uptake of the lighter isotope ^{6}Li, the incorporation of Li into clays and other secondary phases involves either reversible adsorption or irreversible incorporation within the vacant sites of the mineral structural framework.

The process of irreversible incorporation of lithium to the octahedral sheets of smectites, especially at high temperatures, is long known and has been extensively studied. From a structural point of view, the process has been well characterized using analytical tools such as XPS and the Rietveld analysis of neutron scattering data [*Gournis et al*., 2008]. The total occupancy of Li in octahedral positions has been determined by the analyses of the variations on cation exchange capacity (CEC) performed previously and after Li^{+} inclusion to the structural lattice [*Tettenhorst*, 1962; *Schultz*, 1969; *Jaynes and Bigham*, 1987; *Theng et al*., 1997; *Decarreau et al*., 2012]. Uptake of lithium by smectites may occur during the process of clay nucleation and growth (i.e., in hectorite), or by migration from the interlayer to either an octahedral position or to the ditrigonal cavities (i.e., in montmorillonites and beidellites), depending on the charge layer (Figure 1). In both positions, it has been found that Li isotope fractionation occurs [*Williams and Hervig*, 2005], and also Li fractionation can take place at low temperature during the evolution from smectite to illite. Although there

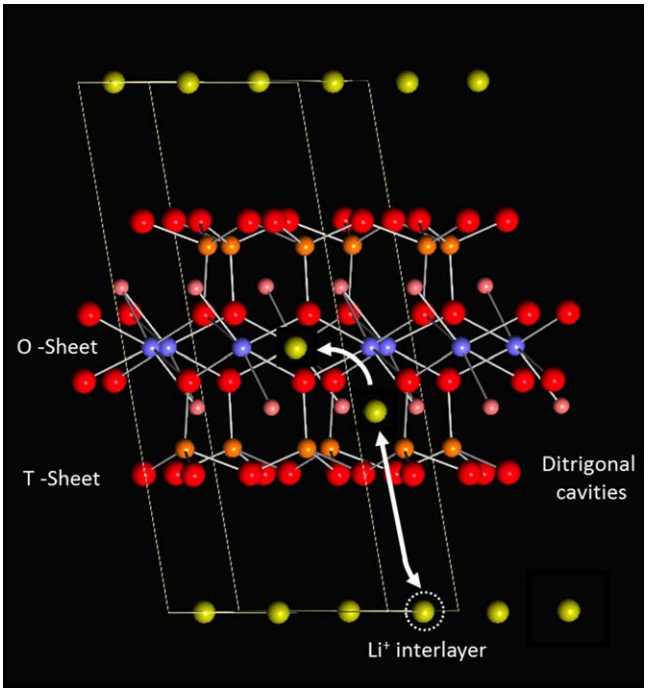

Figure 1. Schematic drawing of the possible sites for lithium uptake by smectites. Li can be incorporated to the octahedral sheets at the nucleation stage, or migrate from the interlayer. It is assumed that only the Li placed in the structural framework, either at the ditrigonal cavities or at the octahedral sites, undegoes isotope fractionation.

has been limited experimental validation of these processes [*Vigier et al*., 2008], it seems that the amount of Li incorporated into the structural framework of clays, and the Li isotope fractionation, cannot exceed a maximum value, whether the concentration of Li in solution increases or not. The experiments detailed in *Vigier et al*. [2008] also show that the Li isotope fractionation factor is linked to the incorporation of Li into the octahedral sites and, although somewhat unexpected, at low temperature ($<$90°C) Li isotope fractionation is quantitatively less important than at high temperature (90–250°C) in smectites (hectorite).

Clay minerals other than smectites (i.e., kaolinite, chlorite, and serpentines) follow different lithium uptake pathways. Kaolinite attracts external cations only by the negative charges of the terminal O^{-2} ions exposed at the edges of the structural sheets [*Carrol*, 1959]. Lithium can be present in solution forming complexes (with the general structure $Li(H_2O)_n^+$) with different hydration numbers, depending on the concentration and pH of the solution [*Jongsik et al*., 2008; *Vorontsov et al*., 2009]. Some of these lithium hydrated species may bond to kaolinite surfaces by forming bidentate inner sphere complexes, leading to Li-isotopic fractionation

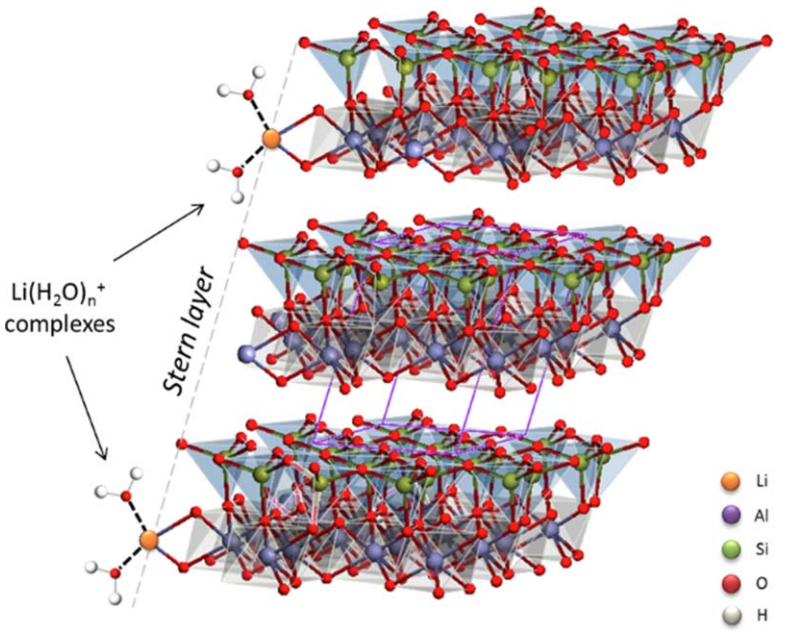

Figure 2. Mechanism of lithium uptake in kaolinite. Li is adsorbed by forming inner sphere complexes that create bidentate bonds with sharing edege octahedra. A similar mechanism is applied to explain Li isotope fractionation on oxyhydroxides and hydroxide surfaces, like ferrihidrite and gibbsite.

(Figure 2). A similar mechanism has also been proposed to explain lithium fractionation in mineral oxyhydroxides and hydroxides (i.e., ferrhydrite and gibssite), while in chlorites and serpentines lithium replaces Mg^{+2} in the brucite layer, a mechanism that also leads to isotopic fractionation [*Wunder et al*., 2010].

All of the mechanisms dealing with Li incorporation into clay minerals mentioned above can be in principle modeled by using algorithms already available in the PHREEQC geochemical code [*Parkhurst and Appelo*, 1999]. Li incorporation into true structural positions of smectites during the processes of nucleation and growth may be considered as a solid-solution forming process between two pure end-members (i.e., Mg-smectite and Li-smectite). This approach has traditionally been applied to analyze the aging process in smectites (i.e., between glauconite and celadonite, to characterize the process of "glauconite maturity" [see, e.g., *Odin et al*., 1988; *Meunier*, 2005]. We use the LLNL (Laurence Livermore National Laboratory) database for all our speciation-reaction calculations.

Here we use the PHREEQC code, and specifically the "Solid Solution" routine (see, e.g., *Parkhurst and Appelo* [1999], for a detailed description). In this approach, the equilibrium between the aqueous phase and the solid solutions is calculated through heterogeneous mass-action equations. The algorithm implemented in PHREEQC uses the Guggenheim equation for determining activities of components in nonideal, binary solid solutions [*Glynn and Reardon*, 1990], which establishes a relation between the saturation constant for a given stoichiometry (K_{ss}) and the excess of free energy resulting from the mixing process:

$$G^E = RT[\ln K_{ss} - x(\ln K_{Ca} + \ln x) - (1-x)(\ln K_{BA} + \ln(1-x))] \quad (1)$$

where G^E (Guggenheim parameter) indicates the excess of free Gibbs energy of the solid solution. From this equation, G^E can be derived using fitting procedures, from experimentally determined K_{ss} constants. Although this is the most formal way to characterize the process of Li incorporation into octahedral sites of secondary minerals, the use of equation (1) becomes difficult in practice, due to the lack of experimental data on the equilibrium constants.

In a similar way, some of the approaches provided in the code to model "surface reactions" may be used to account for ionic diffusion across the diffuse double layer (DDL) or the formation of inner sphere complexes (as we will see in our model cases 2 and 3 below) [*Appelo et al*., 2008]. Even though the use of such specific algorithms could be advantageous for the purpose of a detailed modeling about the specific mechanism of lithium uptake in a particular clay (which is not the aim of this work), the main concern is the lack of experimental data regarding the number of binding sites, size effects of the crystals, kinetic effects, and other issues [*Williams and Hervig*, 2005; *Verney-Carron et al*., 2011]. Practically, the only experimental information available (and not always) about lithium uptake in clays and its isotopic fractionation is the variation on exchange capacity (after the permanent Li incorporation to octahedral sheets) and the measured α fractionation factor.

Assuming these limitations, an alternative way to model Li uptake by clays is the use of an "ion exchange" procedure. For the purposes of this study, this is the more precise procedure, because it relies on available measured data. The main advantage of cation exchange over other algorithms is that the number of exchange sites can be specifically defined, and the amount of lithium exchanged at each position is already available from the literature. In principle, ion exchange does not assume any particular mechanism of lithium uptake and has been interpreted in somewhat different ways in the literature. In a general sense, any replacement of an ion in a solid phase in contact with a solution by another ion can be called "ion exchange" [*Carrol*, 1959]. Cation exchange is, to some extent, an empirical approach that does not assume any particular mechanism of lithium uptake, although the equivalence of this approach with other conceptually different models, like solid-solution algorithms, has been proved by various authors [*Sposito*, 1986]. In clay minerals, this procedure can be used when a cation from solution is exchanged by another cation associated with the clay structure. Although ion exchange is not a chemical reaction in the usual sense, the exchange process is usually written as formally as that of chemical reaction.

We have generated a model accounting for the multisite nature of lithium incorporation in smectites, by considering a two-site model. In this case, the sum of the different sorption sites densities was made equal to the published value of CEC [*Steefel et al*., 2003; *Tertre et al*., 2013]. The Li^+ distribution between solution and smectite is determined by the extent of exchange reactions occurring on the X and Y sites (X = interlayer sites and Y = octahedral sites) that can be defined, using the Gaines-Thomas convection [*Gaines and Thomas*, 1953], as follows:

$$KX + Li^{+} \Rightarrow LiX + K^{+}\ (\text{interlayer sites}) \tag{2}$$

$$MgY_2 + 2Li^{+} \Rightarrow 2LiY + Mg^{+2}\ (\text{octahedral } Mg^{+2},\ \text{e.g., sharing edge octahedra}) \tag{3}$$

where K is an interlayer cation and Mg^{+2} is an octahedral cation on the smectite framework. A mass action law equation, with a constant K, can be defined by:

$$K_{K/Li} = \frac{E_{Li^+}[K^+]\beta_{K^+}}{E_{K^+}[Li^+]\beta_{Li^+}} \tag{4}$$

$$K_{Mg/Li} = \frac{E_{Li^+}\left[Mg^{2+}\right]\beta_{Mg^{2+}}}{E_{Mg^{2+}}\ [Li^+]^2\beta^2{}_{Li^+}} \tag{5}$$

K, the equilibrium constant, determines the reversibility degree of the equation (K = direct rate/reverse rate). Further, only the amount Li^+ in octahedral sites was taken into account for the calculation of isotope ratios in smectites (i.e., the amounts of Li replacing Na or K at the interlayer were not included in the calculations). In a similar way, a single site was defined to take into account the incorporation of Li^+ at the sharing edges of kaolinite, or to model replacement of Mg^{+2} at the brucite layers of chlorite.

2.2. Kinetic Modeling: The Coupling Between Mineral Dissolution-Precipitation and Li Isotope Fractionation

Initial calculations involve the dissolution of basalt under the particular constraints of the model (cooling, evaporation, and pH), allowing us to determine both the ion speciation in solution and the supersaturation state of solid phases and gases. The amount of solids that dissolve or precipitate at each step is then modeled kinetically. Rate expressions used to calculate silicate dissolution were based on the transition state theory [*Lasaga*, 1998], including elementary activity coefficients to model the pH dependency, and the Arrhenius activation factor to constraint the influence of temperature

$$\frac{dm}{dt} = SA\left[K_{H^+} e^{\frac{-E_a}{R}\cdot\left(\frac{1}{T}-\frac{1}{298.15}\right)} a^{n}_{H^+} + K_n e^{\frac{-E_a}{R}\cdot\left(\frac{1}{T}-\frac{1}{298.15}\right)} + K_{OH^-} e^{\frac{-E_a}{R}\cdot\left(\frac{1}{T}-\frac{1}{298.15}\right)} a^{m}_{OH^-}\right](\Omega - 1) \tag{6}$$

where *dm/dt* is the mineral dissolution/precipitation rate (mol/s^{-1}); *SA* is the reactive surface area (m^2); K_{H+}, *Kn*, K_{OH-} are the specific rate constants for dissolution in acidic, neutral, or basic media (mol·m^{-2}·s^{-1}); *R* is the gas constant; and *T* is the temperature (K).

Initially, Li ions are incorporated into solution with the isotopic signature of the parental basalt. As secondary minerals form, incorporation of lithium at the different sites of each mineral is calculated according to the previous ion exchange algorithm applied, and consequently the amount of dissolved Li is lowered. Simultaneous to speciation-reaction calculations, isotope ratios are calculated at each step for every secondary mineral, using a Rayleigh approach included in the PHREEQC code. This is a specific algorithm that permits splitting the total amount of sorbed lithium between ^{6}Li and ^{7}Li isotopes, under the asumption that isotope fractionation occurs following a Rayleigh distillation process [*Zhang et al*., 1998]

$$\frac{R_i}{R_{i-1}} = \left(\frac{C_i}{C_{i-1}}\right)^{\alpha-1} \tag{7}$$

where R_i is the isotopic ratio at the *i*th instant; C_i is the amount Li in solution at the *i*th instant, being $C_i = C_{i-1} - C_{ads,i}$; and α is the isotopic fractionation factor between water and each clay allowed to precipitate or dissolve in the model. α is defined as

$$\alpha = \frac{\left(\frac{^7Li}{^6Li}\right)_{clay}}{\left(\frac{^7Li}{^6Li}\right)_{water}} \tag{8}$$

$\alpha_{clay\text{-}water}$ fractionation factors employed in the model calculations were taken from data available in the literature (Table 1). These include values for kaolinite, smectites, chlorite, illite, and serpentines, as well as for gibbsite and ferrihydrite [*Chan et al*., 1992, 2002; *Huh et al*., 1998; *Zhang et al*., 1998; *Pistiner and Henderson*, 2003; *Williams and Hervig*, 2005; *Teng et al*., 2006; *Vigier et al*., 2008; *Pogge von Strandmann et al*., 2008, 2010; *Millot et al*., 2010; *Wimpenny et al*., 2010; *Wunder et al*., 2010].

Table 1. $\alpha_{clay\text{-}water}$ Fractionation Factors

Group	Phase Name	Half Unit Cell Formula	Charge Distribution (mole/half unit cell) Tetr.	Oct.	Total	CEC (meq/100 g)	Alfa (α)
Kaolinites	Dioctahedral						0.979 [*Zhang et al.*, 1998]
	Kaolinite	$Al_2Si_2O_5(OH)_4$	Charge from broken bonds at edge octahedral			13–15	
	Trioctahedral						
	Amesite	$[(MgFe^{+2})_2Al](SiAl)O_5(OH)_4$	−1	0	−1	13–15	
Smectites	Dioctahedral						0.971–0.999
	Montmorillonite	$(Si_{3.95}Al_{0.05})(Al_{1.36}Fe^{+3}_{0.1}Mg_{0.54}Ca_{0.08}K_{0.075})O_{10}(OH)_2X^{+}_{0.59}$	−0.05	−0.54	−0.59	70–100	[*Wimpenny et al.*, 2010]
	Beidellite	$(Si_{3.4}Al_{0.60})(Al_{1.355}Mg_{0.555}Fe^{+3}_{0.09}Ca_{0.195}Na_{0.18}K_{0.01})O_{10}(OH)_2X^{+}_{1.15}$	−0.60	−0.55	−1.15		
	Nontronite	$(Si_{3.52}Al_{0.30})(Fe^{+3}_{1.8}Al_{0.13}Mg_{0.10})O_{10}(OH)_2X^{+}_{0.307}$	−0.30	−0.10	−0.40		
	Trioctahedral						
	Hectorite	$(Si_{4.00})(Al_{0.02}Mg_{2.65}Li_{0.33})O_{10}(OH)_2X^{+}_{0.33}$	0	−0.31	−0.31	70–100	0.99–1 [*Vigier et al.*, 2008]
Chlorites	Brucite layer						0.984 [*Chan et al.*, 2002]
	Clinochlore	$(Al_{0.76}Fe^{III}_{0.25}Fe^{II}_{0.09}Mg_{4.76})(Si_{0.36}Al_{0.94})O_{10}(OH)_8$	−0.94	0	−0.94	10–40	
	Chamosite	$(Fe^{III}_{0.5}Mg_{1.5}Fe^{II}_3Al)(Si_3Al)O_{12}(OH)_6X^{+}_{0.66}$	−1	0	−1		
Micas	Dioctahedral						0.971 [*Zhang et al.*, 1998]
	Vermiculite	$(Si_{2.895}Al_{1.105})(Fe^{+3}_{0.065}Al_{0.08}Mg_{2.83}Mn_{0.005})O_{10}(OH)_2X^{+}_{0.945}$	−1.105	0.155	−0.95	10–150	
Oxides hidroxides	Ferrihydrite	$Fe^{3+}_2O_3{\cdot}0.5(H_2O)$	Charge from broken bonds at edge octahedral			100–700	0.998 [*Pogge von Strandmann et al.*, 2010]
	Gibbsite	$Al(OH)_3$				100–500	0.986 [*Pistiner and Henderson*, 2003]

In the case of smectites, only an average $\alpha_{smectite\text{-}water}$ fractionation factor value of (0.989–1) is employed, as this is the usually given value in the literature [*Vigier et al.*, 2008; *Pogge von Strandmann et al.*, 2010]. This value was employed in the calculations for all smectites, provided that it was previously reported that these clays incorporate lithium on the structural positions undergoing fractionation, namely, octahedral sheets and ditrigonal positions [*Vigier et al.*, 2008; *Williams and Hervig*, 2005]. This approach was used for the particular case of beidellite, an Al-rich smectite identified on Mars [*Gates et al.*, 2010; *Bishop et al.*, 2010, 2011; *Le Deit et al.*, 2012]. Beidellite represents an intermediate member in the transformation from smectite to illite, which usually forms interstratified structures with montmorillonites. Both clays uptake Li^+ in structural positions [*Tettenhorst*, 1962; *Schultz*, 1969], although with slightly different CEC. In the case of beidellite, a major influence of the tetrahedral charge derived from the replacement of Si^{+4} by Al^{+3} is expected, leading Li^+ to be placed within the ditrigonal cavities and to some minor extent at octahedral sites [*Hofmann and Klemen*, 1950], both structural positions inducing fractionation in smectites.

The amount of Li exchanged at each mineral site dealing with fractionation (i.e., Mg^{+2} in octahedral sheets of smectites) per mineral formula is extended to the total moles of each mineral precipitating in this time step. The opposite applies for dissolving minerals. The net balance of ^{6}Li and ^{7}Li incorporated to minerals by precipitation (or returned to solution by dissolution) is determined, and a new ratio (^{7}Li/^{6}Li) for the dissolution is obtained.

Our results describing Li isotopic distribution in both water and clays are expressed using δ^7Li notation as ‰ deviations from L-SVEC standard [*Flesch et al.*, 1973]:

$$\delta^7\mathrm{Li} = \left[\frac{\left(\frac{^7\mathrm{Li}}{^6\mathrm{Li}}\right)_{\mathrm{sample}}}{\left(\frac{^7\mathrm{Li}}{^6\mathrm{Li}}\right)_{\mathrm{LSVEC}}} - 1\right] \times 1000 \quad (9)$$

This procedure allows iterative calculation of the isotopic composition of the remaining fraction of Li isotopes in water, as well as the Li isotopic signatures of clays resulting from sorption processes. At each time instant, the amount of lithium in solution depends on the balance between the lithium supplied by the basaltic rocks and the rate of uptake/release by clays. Both isotopic signatures are mixed at each modeling step. In a general sense, the procesess leading to a fast dissolution of basalt tends to retain the initial isotopic signature in water by minimizing the δ^7Li enrichment derived from Rayleigh fractionation through "dilution" with the initial basaltic signature [*Vigier et al.*, 2009]. Conversely, those processes generating fast precipitation of clays will favor high δ^7Li values in water [*Pogge von Strandmann et al.*, 2006]. Intermediate

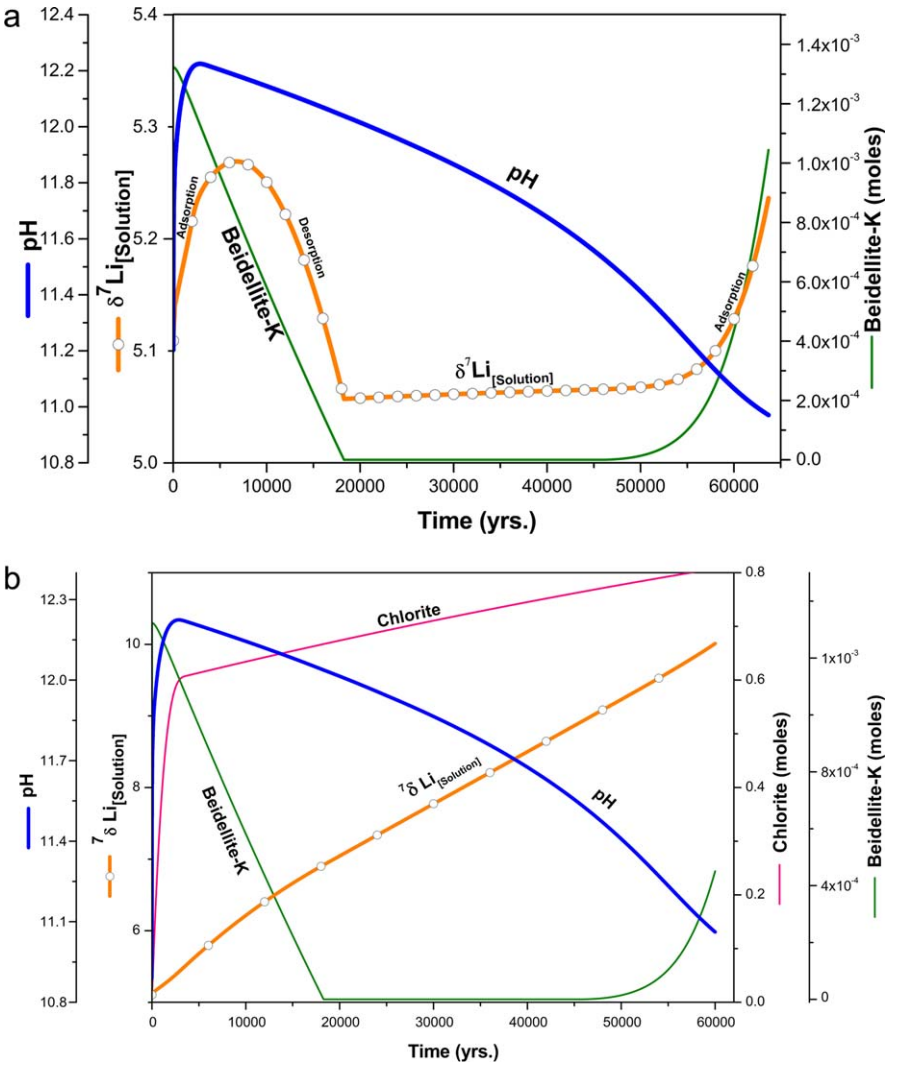

Figure 3. Evolution of δ^7Li in solution during (a) uptake/release of Li during precipitation/dissolution of beidellite and (b) uptake/release of Li during precipitation/dissolution of beidellite and uptake of Li during precipitation of chlorite. The stability of beidellite is determined by the pH of the solution.

situations can arise depending on the particular pathway generating supersaturation: cooling, evaporation, and/or presence of volatiles that can catalyze the pH and redox conditions.

The cooperative effect between growth and the disolving phases together with their specific uptake over the final isotopic signature in the remaining solution is illustrated in Figure 3. For simplicity, we have considered a single system where two clays are precipitating or dissolving: beidellite and chlorite (both typically found on Mars) [see, e.g., *Le Deit et al*., 2012]. In the first case (Figure 3a) it is assumed that only beidellite uptakes Li isotopes, while in the second case both clays are allowed to simultanously uptake lithium isotopes (Figure 3b). Beidellite follows a particular behavior that involves a sequential process of precipitation, dissolution, and again precìpitation as function of the pH of the system. In contrast, chlorite is continuously precipitating along this pH range. If beidellite is the only uptaking phase (Figure 3a), then the curve reflecting the time evolution of δ^7Li tends to mimic the shape of the curve representing the mass amount of clay in the system, although with some delay. This is due to the interplay between uptake and release processes. In fact, even though beidellite is dissolving and releases the light isotope to the solution, the remaining amount of this phase is still adsorbing. As beidellite dissolution continues, release becomes more important than uptake, and the value of δ^7Li in water tends toward recovering the initial isotopic signature of basalt. When both phases uptake lithium simultaneously (Figure 3b), the isotopic composition of δ^7Li in water is

Table 2. Initial Solution[a]

Element Name	Concentration (mol/kg[H_2O])
Al	6.3×10^{-3}
Ca	6.5×10^{-5}
Fe	2.6×10^{-7}
K	3×10^{-5}
Mg	3.1×10^{-3}
Na	3×10^{-5}
Si	8.7×10^{-6}

[a]T = 298.15 K; pH = 8; pe = −6.

continuously shifted toward heavier values, despite the dissolution of beidellite. In a general situation, the isotopic composition of both the solution and clays will depend on the interplay between the whole set of the different phases acting either as sources or sinks of Li, and on the particular trends followed by the system during the weathering process.

In the case studies presented below, it is implicitly assumed that the process of isotopic fractionation starts at t = 0 in all the simulations. Consequently, calculated δ^7Li values are relative values refered to the time period considered in each simulation and are mainly intended to describe relative variation trends, rather than an absolute isotopic signature. In other words, for comparison with a particular system where previous fractionation stages could have ocurred, it would be necessary to use this isotopic signature as the initial value, previous to the processes considered here.

To take into consideration the Li^+ incorporation on smectites to both the interlayer sites and the octahedral sheets, two exchange sites have been defined (Mg^{+2} or Al^{+3} in octahedra; and K^+, Na^+, or Ca^{+2} at the interlayer) for each smectite included in the model. Because lithium adsorbed at the interlayer will not fractionate [*Chevrier et al*., 2007; *Vigier et al*., 2008], only the exchanged Li^+ ions replacing Mg^{+2} at the octahedral sites were taken into account for isotope calculations. Further, to model the kinetic evolution of the process, the net amount of each exchanger X at a site (i) of a particular mineral has been related to the amount of the mineral that dissolves or precipitates according to equation (8), with specific rate constants for each mineral phase.

2.3. Speciation-Reaction and Kinetic Calculations

The starting point of our simulations is a solution in equilibrium with volcanic glass. The resulting dissolution, described in Table 2, is representative of the interaction between the most reactive particles, as basaltic dust and aeolian debris, and was employed as the starting composition at t = 0 for the kinetic calculations in all models. This solution at t = 0 was prepared using an equilibrium calculation, allowing 1 kg of pure water (T = 298.15 K, pH = 7, pe = 4) to instantaneously equilibrate with basaltic glass (saturation index$_{GB}$ = 0). Our simulations start allowing the solution composition described in Table 2 to react with the mineral assemblages listed in Table 3, roughly corresponding to a basaltic andesite as described in *Bandfield et al*. [2000] and *Christensen et al*. [2000, 2004, 2005]. These minerals actually fit the composition of the SNC meteorites and the basalts analyzed in situ by rover investigations at Gale crater, Gusev crater, and Meridiani Planum [*McSween et al*., 2008; *Zipfel et al*., 2011; *Meyer*, 2014; *Schmidt et al*., 2014], and consequently are representative of the average Martian composition. From this moment, the dissolution of primary minerals and the precipitation of secondary phases during the reverse weathering processes were modeled as a function of time, and employing different combinations of the driving supersaturation variables (evaporation, freezing an pCO_2), to generate an array of scenarios where both the sequence of phase development and the evolution of the isotopic signatures can be compared.

To model the kinetics of silicate dissolution and mineral precipitation, we used the values listed in equation (8), which includes the reactive surfaces of the primary minerals (calculated following the geometric model)

Table 3. Rate Constants of Primary Minerals

	Acid Mechanism			Neutral Mechanism			
Mineral Phases	log k[a]	E[b]	n[c]	log k[a]	E[b]	% vol[d]	Surf. Area (1/m)
Anorthite $CaAl_2Si_2O_8$	−3.50	16.6	1.411	−9.12	17.8	56.87	12,680
Enstatite $Mg_2Si_2O_6$	−9.02	80.0	0.600	−12.72	80.0	20.04	3,562
Fayalite Fe_2SiO_4	−4.80	94.4		−12.80	94.4	14.81	1,225
Forsterite Mg_2SiO_4	−6.85	67.2	0.470	−10.64	79.0	8.27	1,644

[a]Rate constant k computed from A and E, 25°C, pH = 0, mol m^{-2} s^{-1}.
[b]Arrhenius activation energy E, KJ mol^{-1}.
[c]Reaction of order n with respect to H^+.
[d]% in the primary mineral assemblage.

[see *Parkhurst and Appelo*, 1999], the specific rate constants, and the dependences on supersaturation, thermal activation energy, and pH. Li isotope calculations were performed at each dissolution-precipitation step. $\delta^7Li_{[solution]}$ results from the balance between the amount of Li supplied by the primary minerals during the dissolution process (thus having the initial isotopic signature) and the selective uptake of Li during the precipitation of variable amounts of secondary phases. Following this procedure, we modeled the different geochemical scenarios described in section 3, with the aim of analizing the influence of the three main factors affecting the solubility of solid phases (dissolved CO_2—through its effect on the pH—evaporation, and cooling) on both the sequence of precipitation of clay minerals and the behavior of the Li isotopes during the process.

2.4. Model Validation From Experimental Data

In order to estimate whether the cation exchange approach used in our calculations correctly reproduce the processes of Li uptake and Li isotope fractionation, we here compare our results with experimental data on isotope fractionation in clays available from the literature. For this purpose, we refer to the experimental work of *Zhang et al*. [1998] who studied the isotope fractionation driven by adsorption of Li from seawater on kaolinite and vermiculite, and determined the corresponding fractionation factors. For the case of smectites, where some amount of Li is incorporated to the octahedral sheets (inducing fractionation) and an additional fraction is sorbed in the interlayer, our model was calibrated based on the experimental work of *Vigier et al*. [2008] on Mg-Li smectites (hectorite).

In the first case, the uptake of Li by secondary minerals was modeled by using the exchange algorithm included in the PHREEQC geochemical code [*Parkhurst and Appelo*, 1999]. Model calibrations were done by using the experimental conditions from *Zhang et al*. [1998]. Comparisons between the isotope fractionation values predicted by the model and those from *Zhang et al*. [1998] were made performing a stepped sequence of rock/water values to reach the final value of 1:20, corresponding to the experimental data reported by *Zhang et al*. [1998]. Modeling for kaolinite and vermiculite was performed in separate runs, and calculations of the resulting δ^7Li in solution were made by using two different procedures. In the first procedure, the total uptake of lithium in the structural positions, inducing fractionation, was used to determine F (the remaining fraction of disolved lithium). The isotope fractionation was further calculated by splitting the total amount of sorbed lithium between ^{6}Li and ^{7}Li isotopes, under the asumption that isotope fractionation occurs according with a Rayleigh distillation process, in terms of delta notation:

$$\delta = (\delta_0 + 1000)f^{\alpha-1} - 1000 \tag{10}$$

In the second procedure, both isotopes ^{6}Li and ^{7}Li were considered in the starting seawater solution, and the selective adsortion of each one on clay mineral surfaces was calculated form the mass action law, by using two separate half reactions:

$$^7Li^+ + X \Rightarrow {}^7LiX \quad (\log\ K = -0.08) \tag{11}$$

$$^6Li^+ + X \Rightarrow {}^6LiX \quad (\log\ K_{kaol} = -0.0713;\ \log\ K_{verm} = -0.0679) \tag{12}$$

where the ratio between the equilibrium constants was constrained to be equal to the alpha factionation factor, given by *Zhang et al*. [1998], and log K values were taken from the PHREEQC database [*Merriam and Thomas*, 1956].

The experimental results reported by *Zhang et al*. [1998] using seawater as the initial solution and R/W weight ratio of 1:20 are compared with the values generated by our model for various parameters: δ^7Li_{sw}, F (the remaining fraction of Li in solution), and the amount of Li incorporated to the mineral phase (μg/g). This procedure was applied to both kaolinite (Figures 4a and 4b) and vermiculite (Figures 4c and 4d). The δ^7Li_{sw} values derived from Rayleigh and equilibrium calculations, based on mass action law, are also compared in Figures 4a and 4c. A similar trend is observed in the two approaches, both in agreement with the experimental data from *Zhang et al*. [1998] until fractionation exceeds a value of approximately $\delta^7Li = 45‰$. For the higher rock/water ratios analyzed in Figures 4a and 4c, the equilibrium model results in systematically lower δ^7Li values than the Rayleigh model. This suggests that at high rock/water ratios, when the number of exchange sites increases significantly in relation to the concentration of lithium in solution, the incorporation of lithium isotopes to the solid phases tends to be less selective, in a similar way as reported

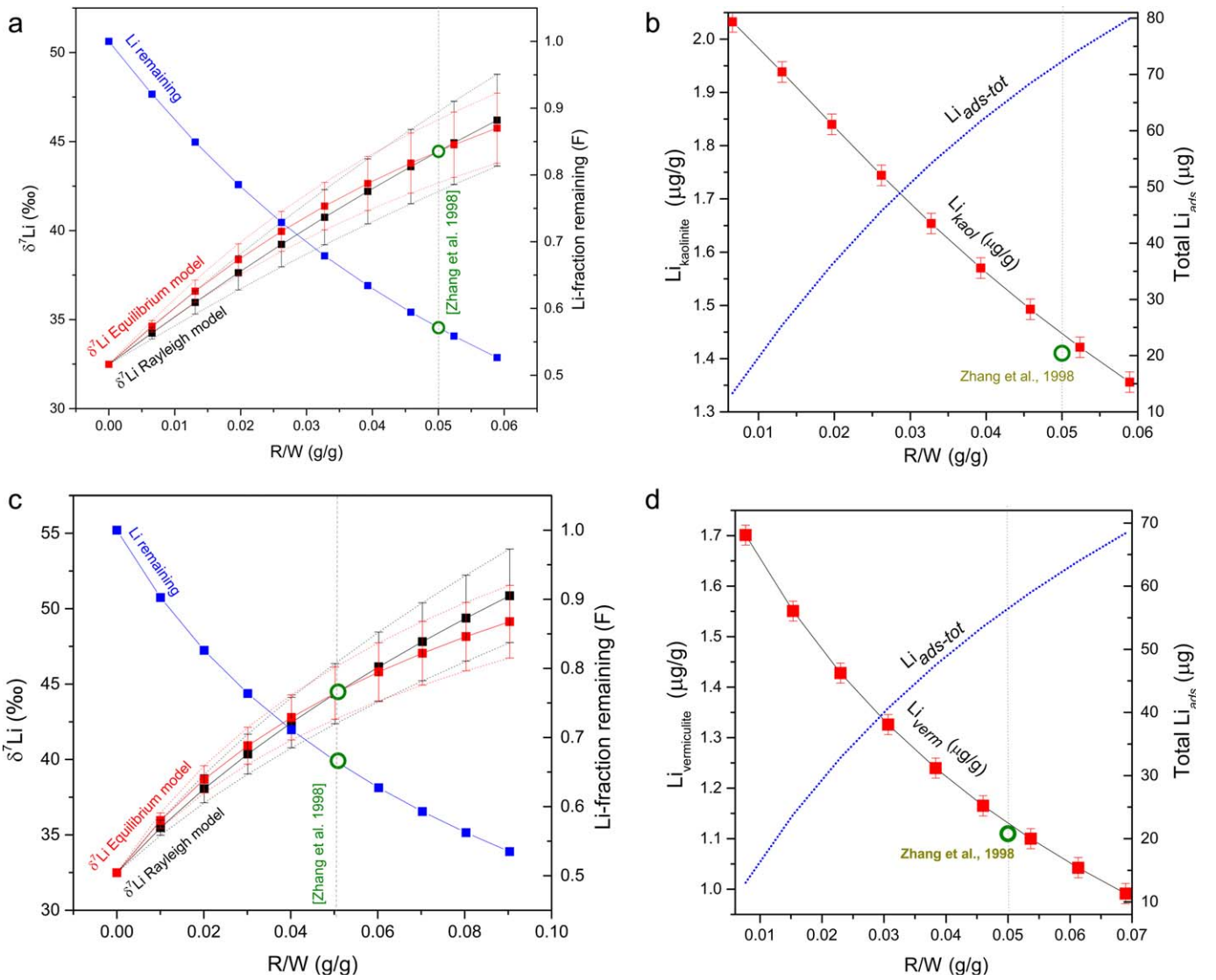

Figure 4. (a) Model calibration for Li isotope factionation in kaolinite based on experimental data from *Zhang et al.* [1998]. Seawater (δ^7Li = 32.4‰) was mixed with kaolinite in variable rock/water ratios. δ^7_{sw} values were calculated either by using the Rayleigh equation or by applying the mass action law to a multisite cation exchange model. The plot also shows the agreement between δ^7_{sw} and the Li remaing fraction (F = 0.5712) with the experimental data from *Zhang et al.* [1998], obtained at R/W value of 1:20. Represented δ^7Li values were obtained by conversion from its original δ^6Li notation. Error bars correspond to the uncertainty associated to the experimental determination of the α constant (α = 1.021 ± 0.004). (b) Amount of Li incorporated to the solid phase (µg/g) derived by the model for different R/W values. The experimental value from *Zhang et al.* [1998], at R/W = 0.05, is also indicated. (c and d) The same as Figures 4a and 4b, but analyzing the case of vermiculite. In this case, the experimentally determined value of the remaining fraction is F = 0.6636, with α = 1.029 (±0.005).

at higher temperatures. Although more experimental work is needed to confirm these aspects, this behavior seems to be consistent with the results from *Williams and Hervig* [2005], which suggest that the degree of fractionation is dependent on the grain size and the reactive surface of the solid phases. In any case, the scenarios considered here involve much lower fractionation degrees, so that both models can be considered as equivalent.

In the second case, to verify that the isotopic fractionation behavior of smectites dealing with irreversible incorporation of Li to their structural framework was correctly described, we used two approaches to model the uptake of Li: a solid solution, and a selective cation exchange at the octahedral sites. The resulting fractionation values were compared with the experimental data. Our calculated model results essentially reproduce the synthesis procedure of hectorite from *Vigier et al.* [2008], where concentrated LiCl solution (20×10^3 ppm Li) was mixed with an amorphous (Si, Al, Mg, and Na) phase with hectorite stoichiometry. In principle, it might be possible to treat the selective incorporation of ^{6}Li to the structural framework of hectorite

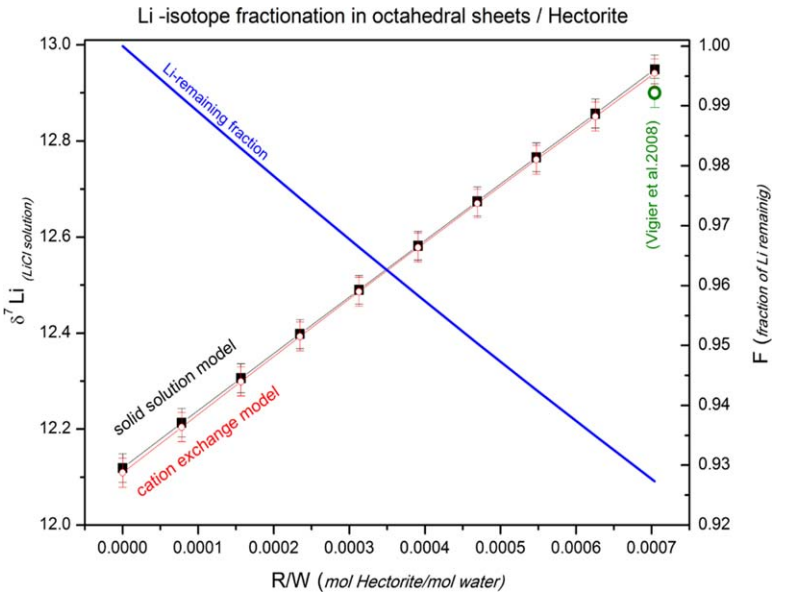

Figure 5. Comparison between Li isotope fractionation in the octahedral sheet of smectites resulting either from a solid-solution approach or from a multisite cation exchange modeling. Both models give almost the same values and agree well with the experimental data reported by *Vigier et al.* [2008] in hectorite. Calculations are made for a 3M LiCl solution ($\delta^7_{ini} \approx 12.1$) during the precipitation of an amorphous gel with hectorite stoichiometry, and at 25°C.

as an ideal solid solution by considering three end-members: pure Mg-hectorite, ^{6}Li-hectorite, and ^{7}Li-hectorite. Alternatively, provided that the ion exchange parameters of the smectite are known, the system could be analyzed as if it would have two set of exchange sites, X and Y, where half-reaction equilibrium constants of each cation is specific for each type of exchange site. In our calculations, we used the values given for log K in the exchange reaction of the PHREEQC database. Model results based on both procedures yield almost identical values for isotope fractionation associated to the incorporation of Li to the octahedral sheets (Figure 5). Equally, these values agree fair well with the *Vigier et al.* [2008] experimental value at 25°C ($\Delta^7 Li_{LiCl(2)\text{-}LiCl(1)} = 0.8$; green circle in Figure 5).

Finally, in order to test the ability of our model to reproduce time-dependent fractionation processes, we have compared the $\delta^7 Li_{solution}$ values calculated with our model with the experimental data obtained by *Wimpenny et al.* [2010] (see Figure 6). *Wimpenny et al.* [2010] used a throughflow batch reactor to analyze Li isotope fractionation during forsterite dissolution, on both far-for-equilibrium and near-equilibrium conditions. In the first case, the solution remains subsaturated, preventing the formation of secondary phases by the continuous removal of solutes. In this situation, *Wimpenny et al.* [2010] noted that no fractionation occurred, and $\delta^7 Li_{solution}$ remains with the same value as that in forsterite crystals ($\delta^7 Li_{forsterite} = 1.57‰$). Near-equilibrium conditions were obtained by decreasing the flux rate in the reactor to promote an increase in the solute concentration and, finally, inducing the precipitation of chrysotile, as a secondary phase. This process drives the Li isotope fractionation. In our model calculations, experimental conditions were as follows: forsterite crystals were assumed to have a BET surface area 800 cm^2/g, Li concentration was 2.05 ppm, and $\delta^7 Li_{forsterite} = 1.57‰$. Our model was run at pH = 10 and T = 273 K, in 0.1 $M_{forsterite}$/kgw. An initial dissolution rate of ($-\log r = 13.8$) was employed. This initial value was allowed to decrease to a value of $-\log r = 14.9$ in order to simulate the drop on forsterite dissolution and on the precipitation of chrysotile at approximately 120 h from the start of the experiment (Figure 6c), caused by the lowering of the flow rate in the throughflow crystallizer. In Figures 6a and 6b, we show the time evolution of $\delta^7 Li_{solution}$ and Li concentration in solution (ppb), calculated with our model and compared with the experimental results from *Wimpenny et al.* [2010], indicating a good agreement of our results with the experimental data.

3. Process-Dependence of Lithium Isotope Fractionation: Case Studies

pH evolution during basalt weathering is mainly determined by the interaction of two factors [*Gislason and Oelkers*, 2003; *Gislason et al.*, 2006]: (1) the silica alkalinity, controlled by the precipitation of clays, and (2)

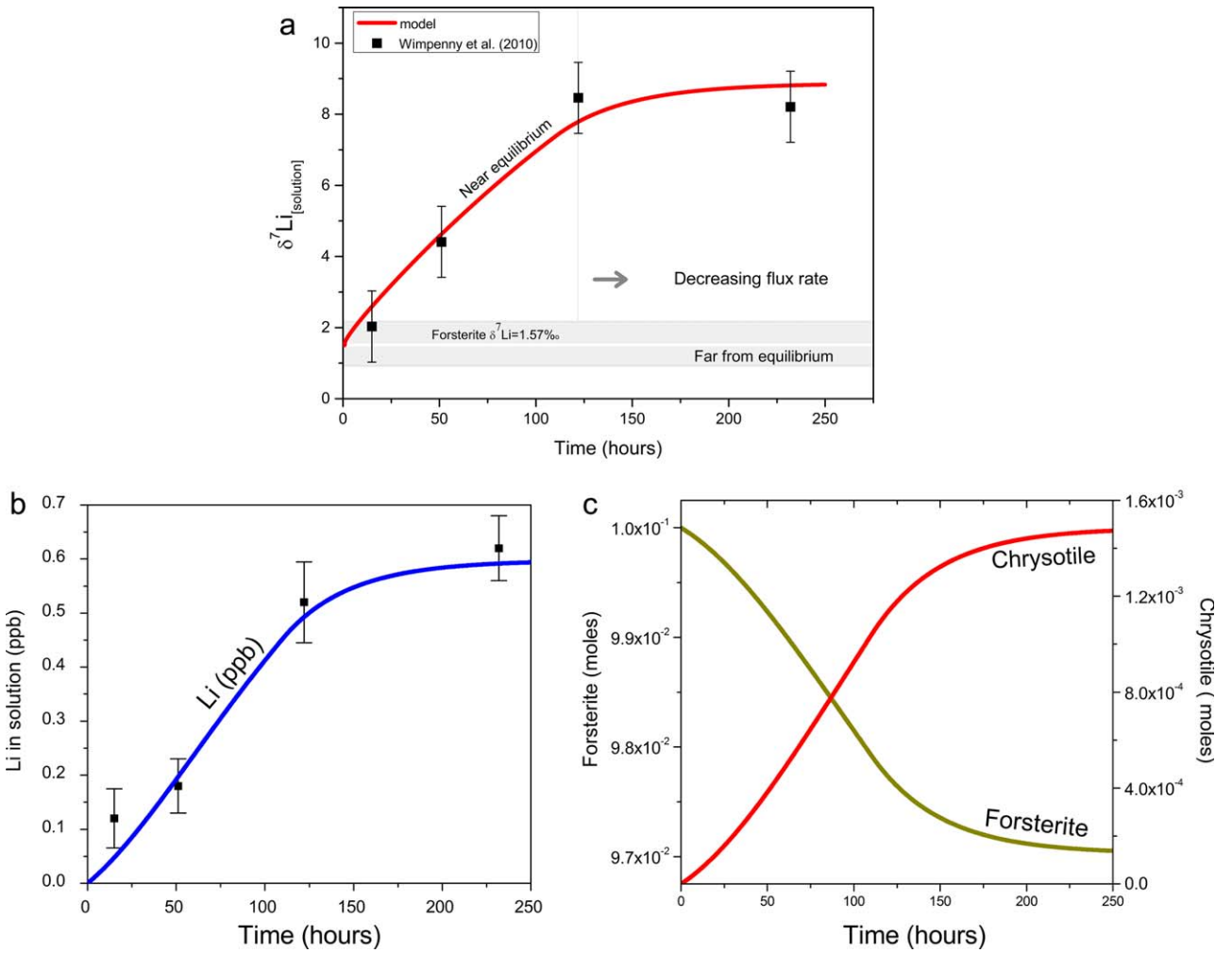

Figure 6. Kinetic evolution of $\delta^7Li_{solution}$ during the dissolution of forsterite at pH = 10, T = 273.15 K. Model results are compared with the data by *Wimpenny et al.* [2010] based on throughflow experiments. (a) Under far-from-equilibrium conditions and continuous removal of reactants, no Li fractionation occurs and $\delta^7Li_{solution}$ remains in the same valor as in solid forsterite ($\delta^7Li_{forsterite} = 1.57‰$) (light gray line). When near-equilibrium conditions are allowed, by decreasing the flow rate, precipitation of chrysotile takes place and induces Li fractionation (red curve). Data points are from the experimental results by *Wimpenny et al.* [2010], and the red line represents our model results. (b) Amount of lithium released to solution. (c) Kinetic of forsterite dissolution leading to the formation of chrysotile as secondary phase.

the carbonate alkalinity, which is driven by the CO_2 speciation. In the absence of CO_2, dissolution of silicates releases Ca and Mg ions to water and promotes the uptake of protons by mineral surfaces, progressively driving the pH to higher values. In this scenario, the rise in pH is only partially counterbalanced by the formation of OH-bearing minerals (i.e., clays, zeolites, and hydroxides). On the other hand, if CO_2 is present, then pH is controlled by the carbonate alkalinity (instead of silica alkalinity) through the interplay between CO_2, HCO_3^-, and $CO_3^=$ species. Precipitation of secondary clay minerals depends on multiple factors such as temperature, pressure, starting basalt, or fluid composition, but the rate controlling step is pH, and pH variations modify both the amount and the type of clays that form [*Stefansson et al.*, 2001]. As the degree of isotope fractionation also depends on the type of clay minerals that precipitate, and their ion exchange capacity, appreciable differences in the isotopic signatures of Li in secondary minerals such as clays are to be expected for each particular thermodynamic and kinetic evolution of the system as a function of pH. Consequently, a detailed study of phyllosilicate abundances and the Li distribution, together with selective Li isotopic analysis on clay minerals, could provide significant insights about the weathering conditions on early Mars. Below we analyze, through geochemical modeling, the expected lithium isotopic composition of both the weathering aqueous solutions and the secondary clay minerals formed under different physicochemical conditions, relevant to the weathering of basalts on early Mars. Our different model scenarios

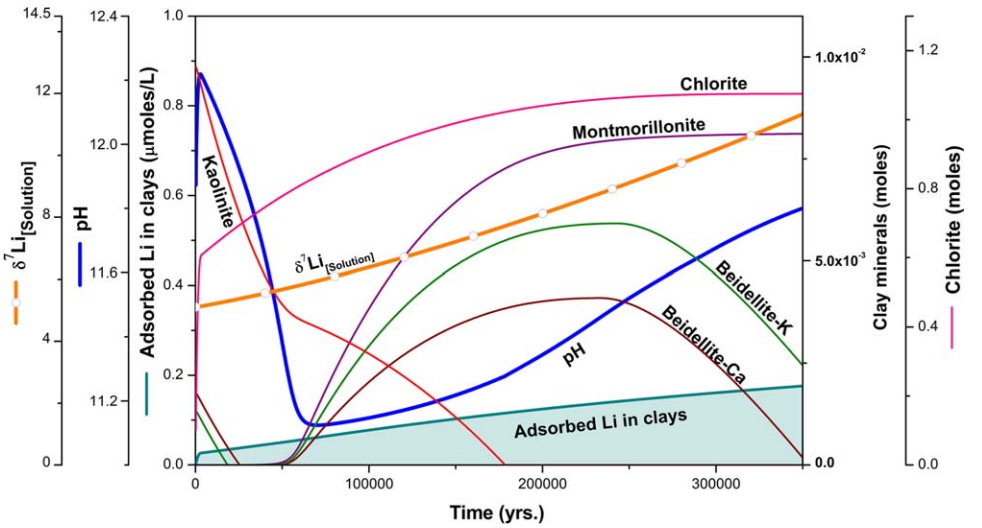

Figure 7. Li-isotopic signature in H_2O resulting from weathering of basalt at near-equilibrium conditions and constant temperature.

include the presence of different CO_2 atmospheres, and therefore our results can provide valuable clues to understand the coeval evolution of the atmosphere and the hydrosphere of Mars.

3.1. Unbuffered Dissolution of Basalt at Constant Temperature (T = 298 K)

To understand the effect of CO_2 on Li isotope fractionation on Mars, first we need to know how Li would behave in the theoretical scenario of the absence of CO_2 in the atmosphere. Therefore, in this first case, we model Li-isotope behavior during the dissolution of basalt at near-equilibrium conditions, when the evolution of the system leads to precipitation of clays at constant temperature (298 K), and with no CO_2. In this model, an initial solution was prepared as previously described in section 2.3. This solution is in equilibrium with basaltic glass (i.e., the saturation index of the basaltic glass is equal to zero), although secondary minerals, compatible with the solution composition, can potentially precipitate. This initial solution is allowed to kinetically react with a crystalline mineral assemblage, and its evolution is monitored through time. We use an initial rock-to-water ratio (R/W) of 2.37 in mass units (g/g), equating to a porosity value of $\phi = 0.57$ that corresponds to a fractured basalt [*McWorter and Sunada*, 1977]. The mineralogical composition, rate constants, and reactive surfaces employed in the calculations are described in Table 3, and the model extends over a time period of 4×10^5 years. In the absence of an external driving force to create supersaturation (i.e., evaporation, cooling, or atmospheric CO_2), the kinetic process is initiated from this starting solution, at t = 0, by the precipitation of secondary clays, using the remaining ions in the initial solution. In turn, this process induces continuous variations of the solution composition, leading to pH variations over time, and modifying at each instant the supersaturation state of both primary and secondary minerals involved in the system. As no external supersaturation variables are applied, the pH evolution of the system is kinetically controlled by the interplay between the precipitation of OH-bearing minerals and the kinetics of dissolution of the primary phases involved in the mineral assemblage of Table 3. An additional, but less relevant, supersaturation source results from the sequestration of water by clays during the sequential precipitation, which tends to keep the system slightly imbalanced over time.

In addition, and provided that lithium isotopes dissolve stoichiometrically, this process yields to an initial isotopic signature of $\delta^7Li_{solution} = 5.1‰$. This case is graphically described in Figure 7. pH rapidly increases at the beginning of the process, from the initial value of 8–12.2, because the fast dissolution of basalt-bearing minerals, especially Ca-plagioclase and, to a minor extent, olivine, which dissolution is kinetically favored at this pH range [*Hurowitz et al*., 2005]. The process simultaneously involves the formation of clay minerals, but as pH increases, some of them (kaolinite, beidellite) become unstable and dissolve. Continuous precipitation of chlorite, a phyllosilicate with a hydroxide (brucite) layer in its structure (and hence stable in highly alkaline conditions), lowers the pH to 11. These conditions once again favor the growth of additional clays, which finally tend to stabilize or dissolve in a process entirely driven by the long-term pH

evolution. In this situation, the Li isotopic signature in solution shows a continuously increasing trend, as is reflected in the δ^7Li curve in Figure 7, promoting a change in the δ^7Li value from 5‰ (the initial signature in basalt) to 12‰ at the end of the time interval considered. This behavior is caused by two main factors: (1) the continuous dissolution of Ca-plagioclase, kinetically favored in such conditions [*Hurowitz et al*., 2005; *Zolotov and Mironenko*, 2007], provides the greatest input of Li to the solution, and (2) the sustained growth of stable clays in alkaline conditions, like chlorite and montmorillonite, which preferentially adsorb ^{6}Li from water and drive the system progressively to a heavier signature through a Rayleigh fractionation mechanism [*Pogge von Strandmann et al*., 2010].

The specific isotopic signatures of different clays (chlorite, beidellite, and kaolinite) are shown in Figure 8. δ^7Li values range in the order of −6‰ to −3.5‰ for kaolinite, −5‰ to 0‰ for beidellite, and −5‰ to 1‰ for chlorite. In the case of kaolinite and beidellite, their isotopic signature becomes progressively heavier until they completely dissolve. This is because Li uptake occurs in water that becomes progressively enriched in ^{7}Li as a result of the Rayleigh fractionation driven by the precipitation of phases such as chlorite and montmorillonite, which ultimately control the Li isotopic signature in solution.

3.2. CO_2-Buffered Dissolution of Basalt During Freezing Processes

A characteristic feature of the kinetics of the dissolution-precipitation of silicates is its pH dependence, which usually leads to graphical representations showing asymmetrically U-shaped curves around neutral pH. These variations in the rate constants are specific for each mineral phase in both primary and secondary silicates. In some cases, dissolution rates are catalyzed by H^+, and at low pH the mineral surfaces become saturated with H^+ so that a further decrease in pH does not cause an increase in dissolution rate [*Palandri and Kharaka*, 2004]. The evolution of Li isotopic signatures is very dependent on pH, because it depends on the balance between the amount of ^{6}Li derived from the dissolution of primary minerals and the amount of secondary minerals involved in the selective uptake of ^{6}Li. Assuming that dissolved CO_2 was the most relevant factor triggering pH changes in the early Martian environments [*Fairén et al*., 2004], we now analyze the influence of transient and long-term atmospheres, including CO_2, on the rates of silicate dissolution. We model different situations including the effect of simultaneous evaporation and cooling, which are the two additional variables that affect supersaturation.

3.2.1. Buffering by a Limited Amount of CO_2 That is Finally Consumed

In this scenario, we model the effects of a thin and transient CO_2 atmosphere, in a simulation extending up to 10^3 years. We assume a thin atmosphere similar to the one existing today ($\log_P CO_2 = -6$ atm), and a limited amount of CO_2 (g) entering the system at a constant rate (zero-order rate, $K = 5 \times 10^{-5}$ mol/L yr) during the initial 200 years. A simultaneous continuous cooling process during 200 years lowers the temperature of the system from 298.15 K down to 243 K, and then the temperature keeps constant during the remaining 800 years of the simulation. The CO_2 (g) partially dissolves in water, at increased rates during the cooling process due to its inverse solubility on temperature. This CO_2 (g) forms different species depending on the pH (CO_2(aq), HCO_3^-, $CO_3^=$), or is consumed by carbonation reactions. We assume the same initial solution, rock-to-water ratio R/W = 2.37 (g/g), mineral assemblages and reactive surfaces that in the previous case (described in Tables 3 and 4). The low ionic strength of the initial solution results in a freezing point depression of a few degrees, inducing the instantaneous formation of ice at temperatures below 271 K. Ice would float and aggregate forming an upper cover, and the salt segregation would induce a considerable increase of the ionic strength of the remaining solution that progressively reduces the freezing point depression of the residual water. With time and continued cold, the ice layer would get thicker [*Fairén et al*., 2011].

In this model, the pH of the system fluctuates slightly from alkaline toward circumneutral values, to eventually return to the alkalinity. Figure 9 shows the sequential precipitation of clays during the weathering of basalt. As observed on the left side of Figure 9, the pH decreases in a process driven primarily by the CO_2 speciation in water along with the OH uptake by silicate layers. The result is the initial formation of significant amounts of clays. Unlike the situation described in Figure 7, in this case, beidellite and kaolinite are kinetically favored and form in amounts greater than chlorite. As temperature falls to 240 K and the supply of CO_2 ceases, the system slowly shifts again toward high pH values. During this period, the amount of clays remains nearly stationary. This is due to both the solubility trend of clays with temperature and the higher activation energies required at low temperature to permit clay growth.

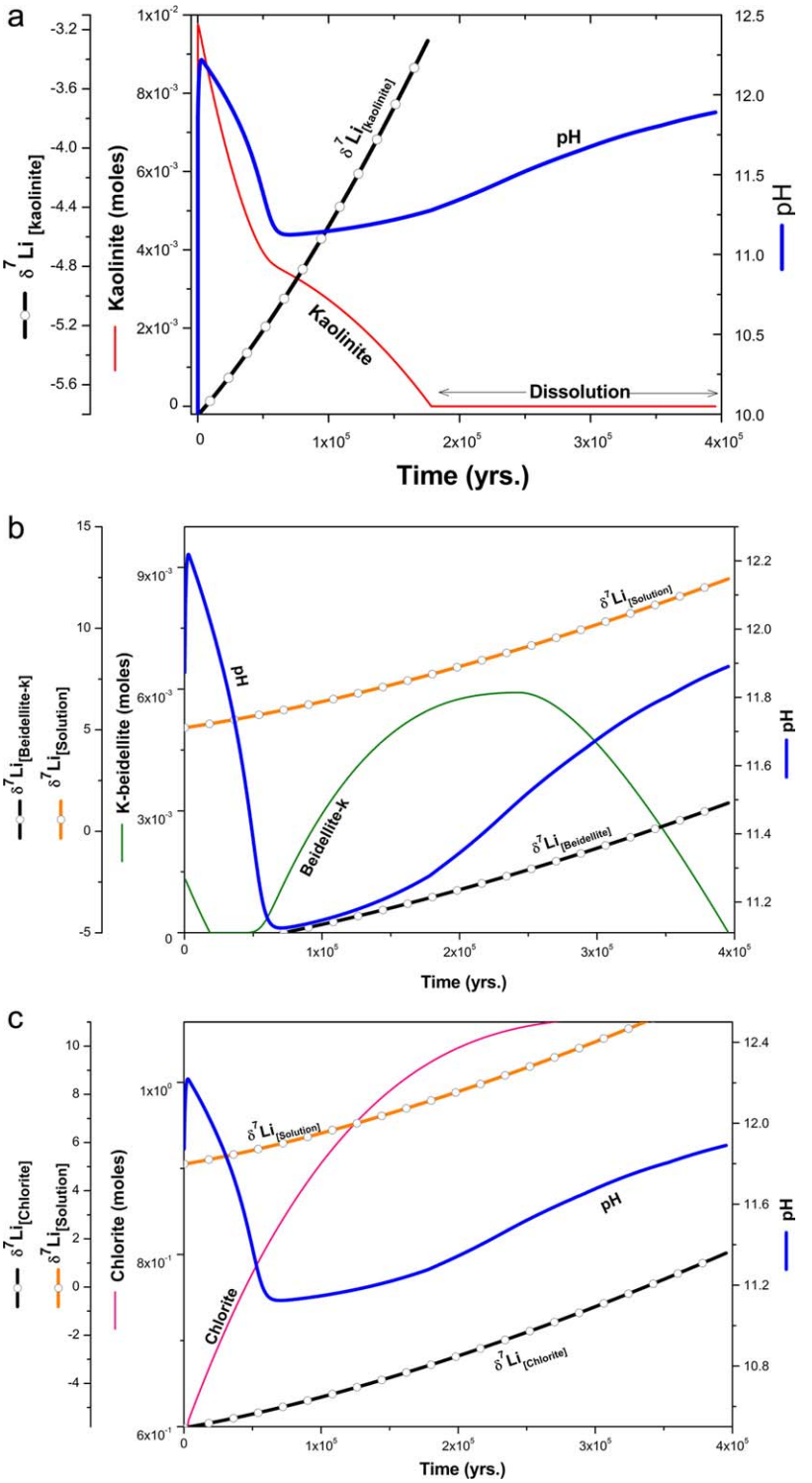

Figure 8. Li-isotopic signatures of Kaolinite, K-beidellite, and chlorite from the model in Figure 7, showing their dependence on the kinetics of clay precipitation/dissolution and on pH. The evolution of $\delta^7Li_{solution}$ is also shown for comparison.

The specific variations of δ^7Li in different clays (chlorite, beidellite, and kaolinite), compared with the corresponding δ^7Li values in solution, are shown in Figure 10. In this case, the isotopic enrichment leading to the heavier δ^7Li value in water is mainly due to beidellite formation, and to a minor extent to kaolinite formation, as evidenced by the fact that the amount of these clays and their δ^7Li values follow analogous trends

Table 4. Rate Constants of Secondary Minerals

	Acid Mechanism			Neutral Mechanism		Basic Mechanism		
Mineral Phases	log k[a]	E[b]	n[c]	log k[a]	E[b]	log k[a]	E[b]	n[c]
Beidellite[d] $Na_{0.5}Al_{2.5}Si_{3.5}O_{10}(OH)_2{\cdot}(H_2O)$	−11.31	65.9	0.777	−13.18	22.2	−17.05	17.9	−0.472
Chamosite-7A $Fe_3^{2+}Mg_{1.5}AlFe_{0.5}^{3+}Si_3AlO_{12}(OH)_6$	−10.98	23.6	0.340	−12.78	35.0	−16.52	58.9	−0.400
Clinochlore-14A $(Mg,Fe^{++})_5Al(Si_3Al)O_{10}(OH)_8$	−11.11	88.0	0.500	−12.52	88.0			
Smectite[e] $K_{0.04}Ca_{0.5}(Al_{2.8}Fe_{0.53}Mg_{0.7})(Si_{7.65}Al_{0.35})O_{20}(OH)_4$	−10.98	23.6	0.340	−12.78	35.0	−16.52	58.9	−0.400
Kaolinite $Al_2Si_2O_5(OH)_4$	−11.31	65.9	0.777	−13.18	22.2	−17.05	17.9	−0.472
Brucite $Mg(OH)_2$	4.73	59.0	0.500	8.24	42.0			
Nontronite-Mg[f] $Na_{0.3}Fe_2^{3+}Si_3AlO_{10}(OH)_2{\cdot}4(H_2O)$	−12.71	71.0	0.220	−14.41	48.0	−14.41	71.0	−0.130
Gibbsite $Al(OH)_3$	−7.65	47.5	0.992	−11.5	61.2	−16.65	80.1	−0.784
Glauconite $K_{0.6}Na_{0.05}Fe_{1.3}^{3+}Mg_{0.4}Fe2+_{0.2}Al_{0.3}Si_{3.8}O_{10}(OH)_2$	−4.80	85.0	0.700	−9.1	85.0			
Montmorillonite $K_{0.318}(Si_{3.97}5Al_{0.025})(Al_{1.509}Fe_{0.205}Mg_{0.283})(OH)_2$	−12.71	48.0	0.220	−14.41	48.0	−14.41	48.0	−0.130

[a]Rate constant k computed from A and E, 25°C, pH = 0, mol m^{-2} s^{-1}.
[b]Arrhenius activation energy E, KJ mol^{-1}.
[c]Reaction order n with respect H^+.
[d]Kinetic constants based on smectite values.
[e]Kinetic constants based on kaolinite values.
[f]Kinetic constants based on montmorillonite values; E_a values, from *Osthaus* [1954].

to δ^7Li in water. Chlorite is unstable in this case and, although it tends to dissolve, its isotopic signature is controlled by the Rayleigh fractionation induced in the water by the formation of other clays.

In this scenario, fluctuations of pH around circumneutral values promote two different trends for $\delta^7Li_{[solution]}$ evolution. As is observable in the left part of Figure 9, during the pH decrease, $\delta^7Li_{[solution]}$ increases and progressively tends to a stationary value. This is because, although the evolution of pH to circumneutral values favors the formation of clays, it also induces the simultaneous dissolution of primary silicates, leading to a greater amount of Li in solution with the low isotopic signature of primary minerals ($\delta^7Li = 5.1$). This behavior acts as a framework condition for Rayleigh fractionation, and consequently diminishes its ability to reach heavy isotopic signatures. As pH rises again toward more alkaline values, the kinetics of both dissolution and growth tends to slow down, in a process aided by the cooperative effect of low temperature.

The pH-dependent behavior of the Li isotope fractionation is by far more noticeable when pH fluctuations proceed more slowly. For example, assuming the same conditions than in the previous model, except considering a rate of CO_2 supply 10 times lower, the process extending over 10^5 years, and occurring under conditions of simultaneous freezing and evaporation (Figure 11a), then $\delta^7Li_{[solution]}$ approaches a stationary value at about 5×10^3 years.

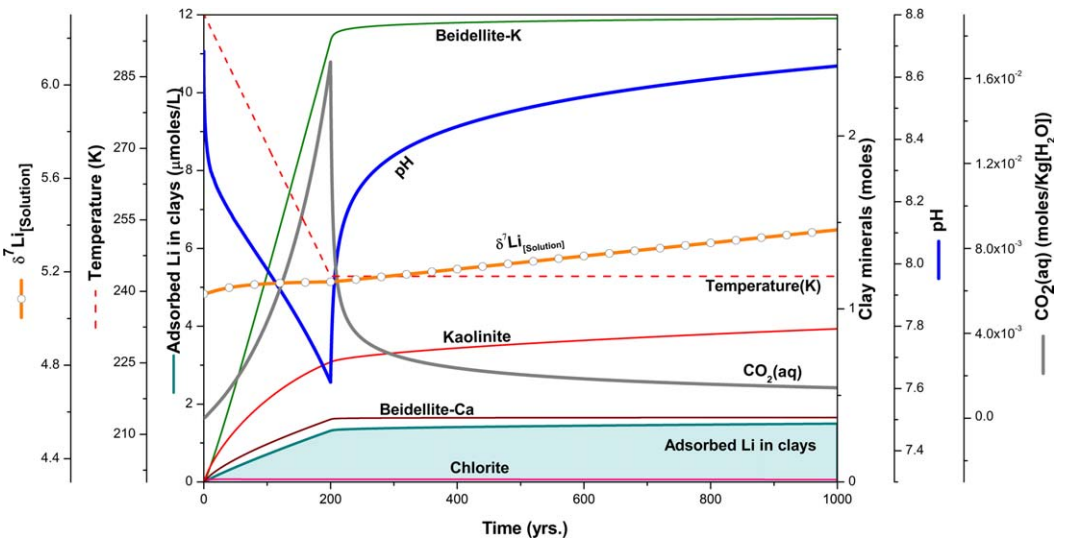

Figure 9. Evolution of δ^7Li in a system subjected to cooling and transitionally buffered by CO_2.

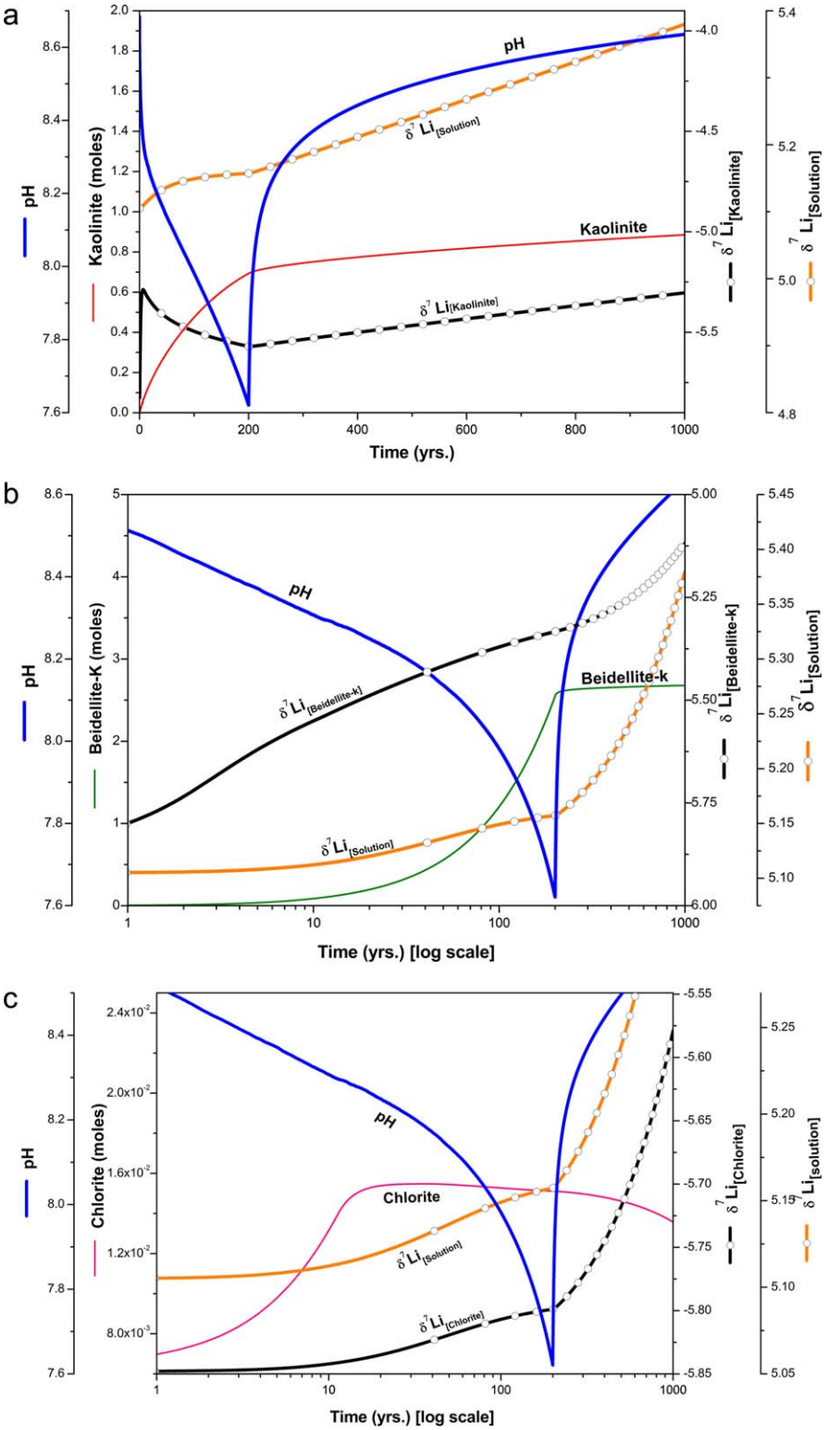

Figure 10. Comparison between $\delta^7Li_{solution}$ and δ^7Li_{clay} for kaolinite, K-beidellite, and chlorite in the model of Figure 9, showing its dependence on the kinetics of clay precipitation/dissolution and on pH.

A detailed review of the parameters involved in this scenario is shown in Figure 11b. We have plotted the dissolution-precipitation kinetics of minerals with faster and slower pH fluctuation, together with the amount (mol) of mineral precipitated versus mineral dissolved, and also together with the ratio of Li

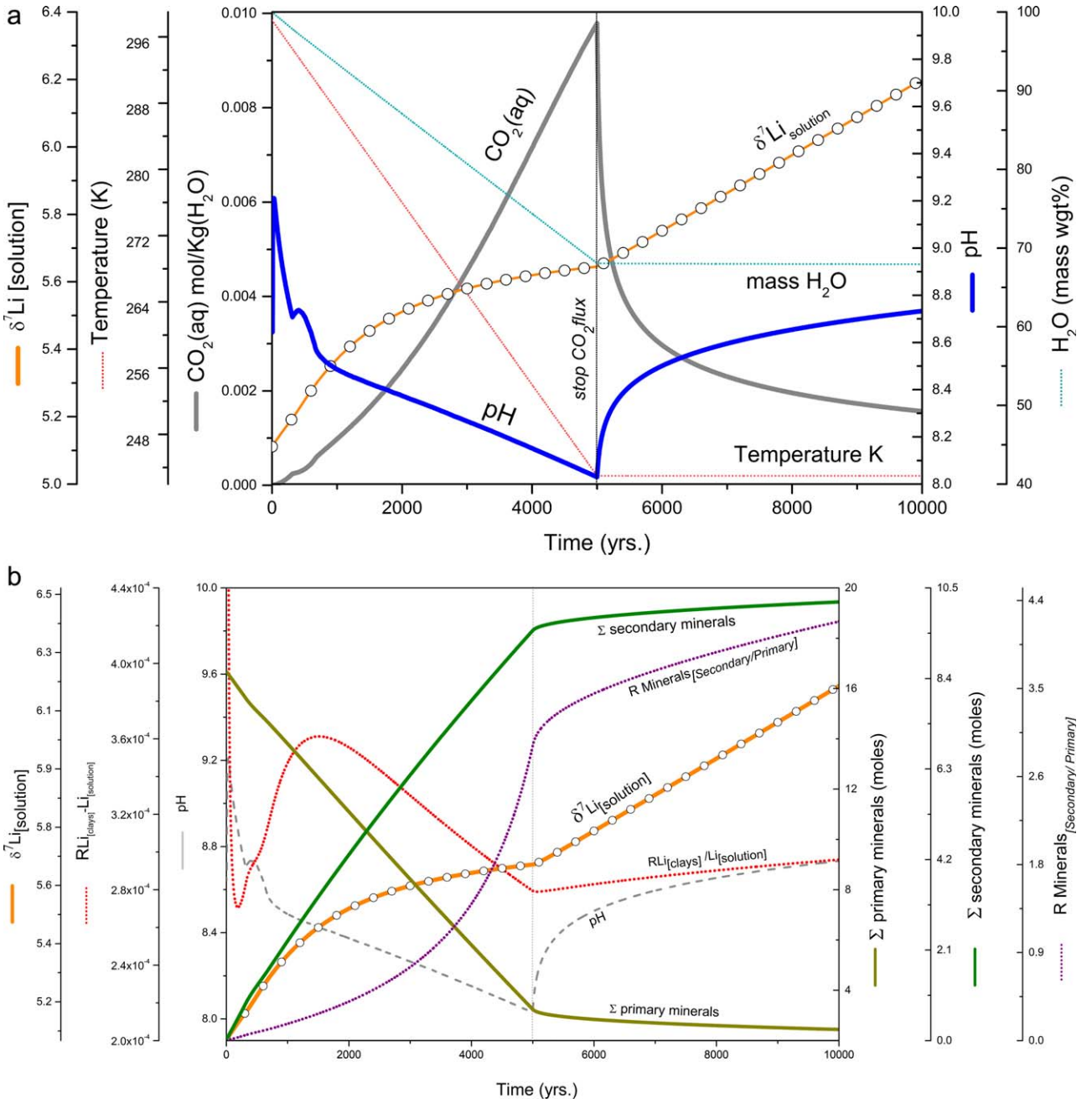

Figure 11. δ^7Li evolution during pH fluctuations induced by episodic changes in $CO_{2(g)}$ considering simultaneous evaporation and cooling. (a) As the pH goes down from 9 to 8, the $\delta^7Li_{[solution]}$ growths and tends to a stationary value, as result of the enhanced dissolution-precipitation process. As the pH raises toward alkaline values, the kinetics of dissolution-precipitation slows down because the cooperative effect of low temperature and evaporation, resulting in a linear trend of $\delta^7Li_{[solution]}$. (b) Dissolution-precipitation kinetics of primary and secondary minerals on both sides of the pH fluctuation. The ratios (in moles) of mineral precipitation/dissolution, and the Li incorporated into clays versus Li in solution, are also shown on both sides of pH fluctuation.

incorporated into clays versus Li released from basalt. During the first stages of evolution, pH decreases from >9 to 8, and dissolution and precipitation follow markedly opposed trends. When pH rises again and the system deviates from circumneutral values, the amount of primary and secondary minerals remains nearly constant. Nevertheless, the growth of secondary phases is slightly favored, as marked by the positive trend of both the ratio of mineral precipitated versus mineral dissolved and the ratio of Li incorporated into clays versus Li released from basalt. In the end, a positive (nearly linear) evolution of $\delta^7Li_{[solution]}$ can be

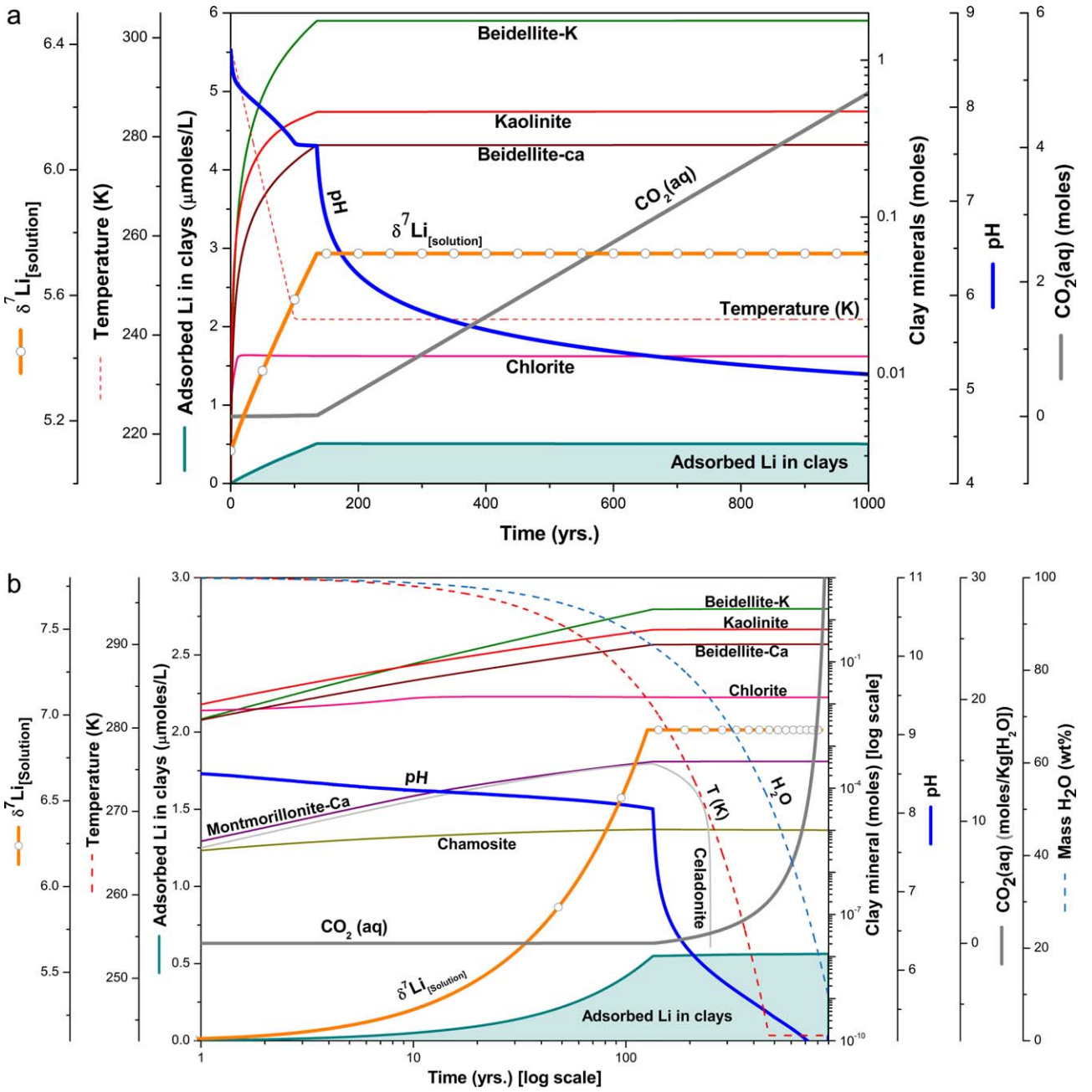

Figure 12. δ^7Li evolution with a continuous supply of CO_2 under (a) cooling conditions and (b) simultaneous cooling and evaporation. (c) Summary of the main parameters included to analyze the behavior of δ^7Li in the case of Figure 12b: at pH slightly over 8, both the amount of secondary minerals and the uptake of lithium from solution rapidly increase. When pH drops toward acidic values, the precipitation of clays become unfavorable and the supersaturation of the system reaches a stationary value. Eventually, the dissolution of primary minerals ends and δ^7Li becomes constant.

observed, and the slope depends on the duration and intensity of pH fluctuations induced by the episodic CO_2 outgassing.

3.2.2. Buffering by a Stable CO_2 Atmosphere Under Simultaneous Cooling and/or Evaporation

In this scenario, we model the effects of a long-term and denser CO_2 atmosphere, which has been proposed to have existed on early Mars [e.g., *Fairén et al.*, 2004, 2009, and references therein]. Unlike the previous case where pH variations from alkalinity toward circumneutral values were modeled, in this case we assume that CO_2 outgassing proceeds continuously, leading the system to reach acidic conditions in the long term [*Fairén et al.*, 2004]. Model conditions are the same as in the previous case, except for the fact that the rate of

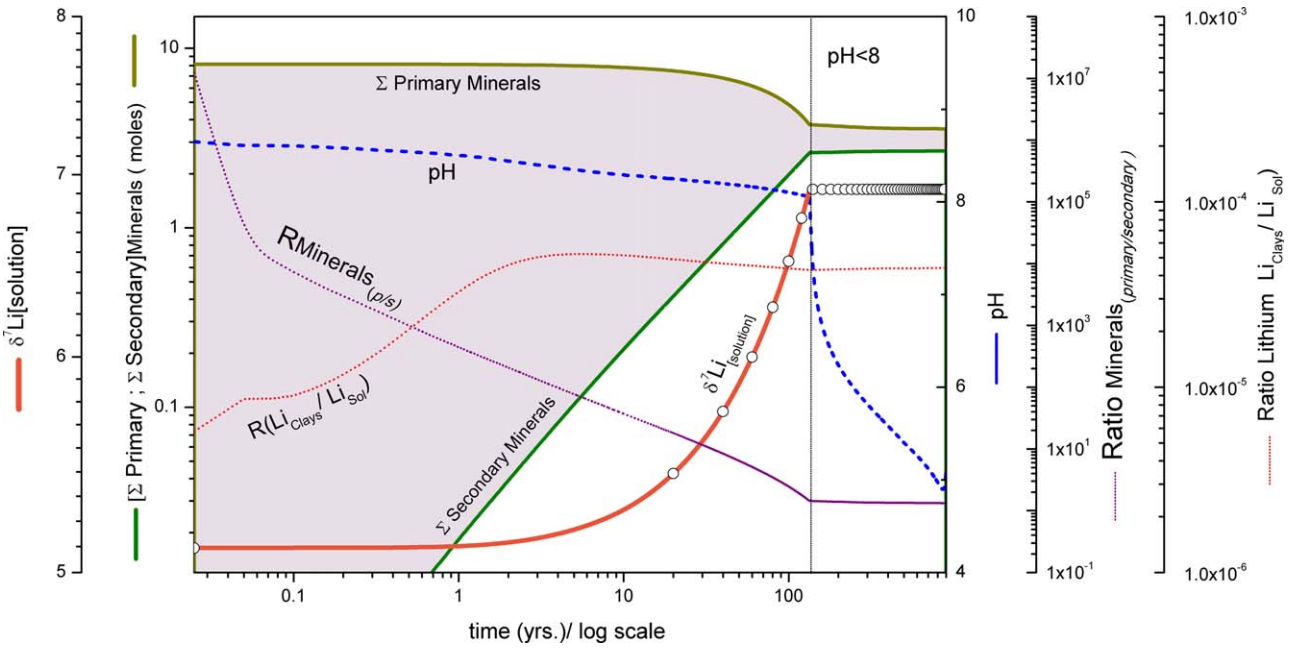

Figure 12. (continued)

CO_2 (g) supply is 5×10^{-3} mol/L yr, during the whole 10^3 model years. Initially, the pH decreases slowly, controlled by the balance of hydroxyl groups derived from the dissolution and precipitation of minerals. Also, as in the previous case, CO_2 (g) dissolution is progressively enhanced during the cooling process, allowing the formation of solution species depending on pH. However in this case, when the system reaches acidic pH values, the presence of CO_2 (aq)—the more stable species in this pH region—is favored over the deprotonated species (HCO_3^-, $CO_3^=$), and consequently a progressive increase in the concentration of CO_2 (aq) is expected.

In this situation (Figure 12a), clay minerals formation takes place at the early stages of the process, during cooling. The process of clay formation is mainly driven by pH decreasing to neutral values. Consequently, δ^7Li in solution continuously increases during this period as result of the progressive uptake of ^{6}Li to clays. As the system drops to acidic pH values, the formation of new clays become not favored, and the continuous supply of Li from basalt with a light isotopic signature makes the net increase in δ^7Li small. When the system reaches the lowest temperature value ($\sim$245 K), the amount of clays in the system tend to a steady state that possibly reflects the combined effect of temperature and the acidic pH values. In the end, Li uptake by clays ceases and $\delta^7Li_{[solution]}$ reaches a stationary value (5.7‰).

If evaporation acts as an additional source of supersaturation, then the observed path is essentially the same, although the stable value of $\delta^7Li_{[solution]}$ is higher (Figure 12b). This is because evaporation increases the precipitation of secondary minerals (i.e., clays), but does not increase the dissolution of primary minerals (i.e., basalt). In consequence, the amount of Li with low isotopic signature supplied by the primary minerals remains constant, thereby improving the efficiency of the Rayleigh process which leads the system toward heavier $\delta^7Li_{[solution]}$ values. A summary of this model scenario is shown in Figure 12c. When pH values are $>$8, the amount of secondary mineral precipitation rapidly increases, as well as the uptake of lithium from solution. This is reflected in the curve representing the ratio of Li in clays versus Li in dissolution in Figure 12c. When the pH falls below 8, evolving toward acidic values, the precipitation of clays become unfavorable. When precipitation of clays is no longer a sink for ions, the dissolution also ends, leading as consequence to a nearly stationary value of $\delta^7Li_{[solution]}$.

4. Discussion

4.1. Lithium Isotope Fractionation Pathways

The scenarios discussed in section 3 enable us to identify particular trends concerning the evolution of δ^7Li during basalt weathering as a function of the driving mechanisms that interact to create supersaturation

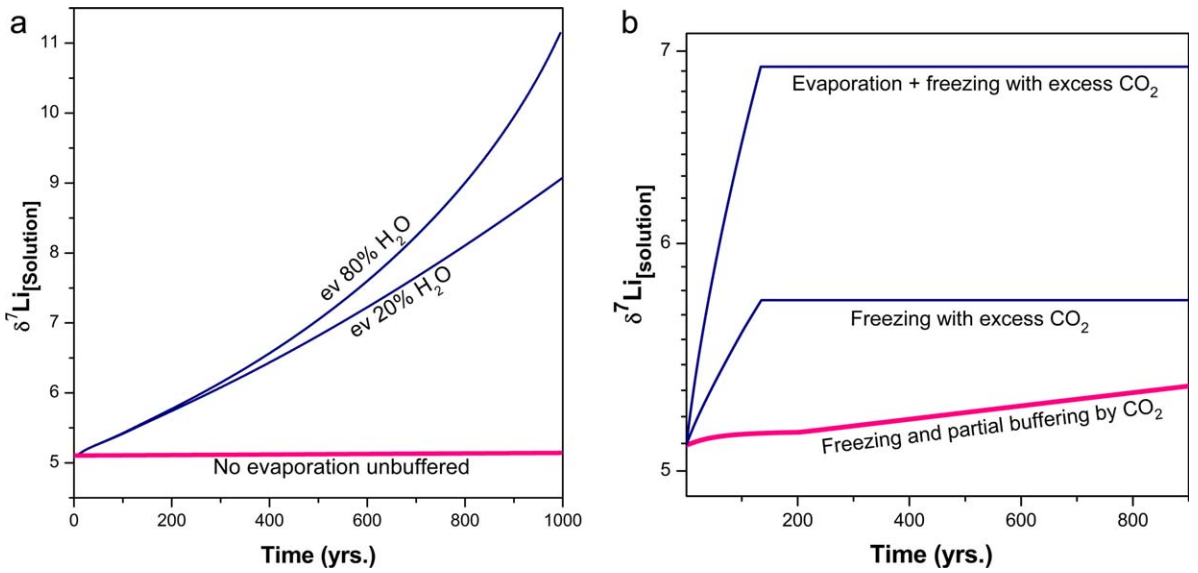

Figure 13. Lithium isotope fractionation pathways. (a) Starting from a process at 298 K, when supersaturation is created by evaporation of different amounts of water. (b) Evolution in presence of CO_2, when supersaturation is created either by cooling or simultaneously by cooling and evaporation.

(evaporation and/or cooling), together with those relevant to modify the pH (CO_2 or other volatiles), thus influencing the balance between silicate dissolution and secondary mineral precipitation.

In the absence of CO_2 and without evaporation or cooling effects (Figure 13a), the release of cations by silicate mineral dissolution proceeds slowly. The main control on secondary mineral stability comes from pH and cation supply. As both growth and dissolution processes are counterbalanced, Li does not accumulate in solution, and Rayleigh fractionation due to secondary mineral formation is an efficient mechanism—although slow—to progressively increase the δ^7Li value of the water in the long term. This effect can be enhanced if other processes promote supersaturation, e.g., evaporation. Evaporation can notably enhance the formation of secondary minerals, without significantly changing the rate of cation supply. Consequently, as the amount of dissolved Li is nearly constant and uptake of Li increases with clay precipitation, the δ^7Li value of the solution shifts to higher values.

For basaltic environments in contact with atmospheric volatiles, pH is the rate controlling step in the formation of secondary phases (Figure 13b). Clay minerals such as kaolinite and beidellite (pervasively identified on Mars [see, e.g., *Bishop et al*., 2010, 2011; *Le Deit et al*., 2012; *Ehlmann et al*., 2013]) are oversaturated at circumneutral pH and tend to be unstable at pH values greater than 9 [*Stefansson et al*., 2001]. In contrast, chlorite and montmorillonite (also largely reported to be present on the surface of Mars [see, e.g., *Mustard et al*., 2008; *Le Deit et al*., 2012; *Ehlmann et al*., 2013]) are more stable at high pH values [*Pogge von Strandmann et al*., 2010]. In the presence of CO_2, an initial pH decrease tends to favor the formation of clays, but also the dissolution of primary minerals. In addition, in the absence of cooling, δ^7Li is expected to increase as pH decreases to near neutral values, although this effect will be to some extent minimized by the increase of Li in solution with an initially lighter isotopic signature. The final pH value will depend of the interplay between the alkalinity, driven by the rate of dissolution of primary silicates, and the buffering effect of carbonate species. When cooling is considered, the formation of secondary clays almost ceases because of Arrhenius' dependency of the growth rate [*Fairén et al*., 2011], hence leading to a stationary value of δ^7Li. The final isotopic signature could be greatly influenced by the amount of time the system remains at higher temperatures and neutral pH values. In addition, as in the previous case, a heavier isotopic signature in solution will result if an evaporative regime takes place simultaneously to the cooling process.

A particularly differential aspect of basalt weathering on Mars compared to Earth might have been the specific role played by simultaneous evaporation and cooling over the number and type of secondary minerals forming. For example, as noted above, low-temperature weathering can lead to the formation of small

amounts of clays as consequence of the Arrhenius activation energy for crystallization [*Fairén et al*., 2011]. Therefore, the isotopic signature (δ^7Li) of the resulting clays is expected to be very low in Martian weathering environments. The simultaneous role of evaporation and freezing notably modifies the sequence of precipitation of secondary phases. Hence, comparative analyses between the secondary minerals undergoing fractionation and those retaining the δ^7Li water signature at the moment of crystallization (i.e., Li incorporated to sulfates) may provide important information about the geochemical evolution of the surface of Mars.

4.2. Strategies for Future Analyses

Neither MSL nor any other previous mission to Mars can perform an analysis of Li isotopes. MSL includes a Laser-Induced Breakdown Spectrometer (LIBS) intrument as part of the ChemCam suite investigation. ChemCam is very sensitive to Li; however, the isotopic separation of atomic emissions for Li is too narrow: 0.015 nm at 670 nm versus ChemCam's resolution of 0.65 nm at the same wavelength. So there might be a slim possibility of seeing a molecular isotopic effect if ChemCam hits a nearly pure Li oxide (B isotopes can be detected with LIBS that way [*Russo et al*. [2011]), but that is improbable for MSL. MSL also includes a gas chromatograph/mass spectrometer as part of the SAM suite investigation, intended to detect and characterize the isotopic composition of volatiles released from vaporized soil and rock samples by heating. But as Li compounds are not volatile, SAM would be unable to analyze Li isotopes.

As we have shown in this paper, a detailed analysis of the Li isotopic ratios in secondary mineral lattices could provide important clues about past weathering conditions on Mars with respect to weathering extent, temperature, pH, and supersaturation or evaporation rate of the initial solutions in contact with basalt rocks. To perform such analyses, it is necessary to develop strategies for future identification and collection of Martian materials that could be used to investigate aqueous processes via study of Li isotope fractionation patterns. To that end, we suggest that future surface robotic explorers on Mars may include an instrument payload capable of supplying all the relevant data. The payload must include (1) an instrument that can perform selective mineralogical analyses, such as an X-ray diffraction (XRD) instrument; (2) an instrument capable of detecting trace amounts of Li in minerals, such as a LIBS instrument; and (3) an instrument that can perform selective isotopic analyses, including Li isotopes. Alternatively, sample collection and return missions being currently developed (such as Mars2020) may focus in the identification and collection of samples containing Li, which would eventually be analyzed in Earth laboratories. The minerals that would preferentially adsorb Li would be the main target for the prospect isotopic analysis and for testing the models described here, as the amount of adsorbed Li in a secondary mineral will also vary in function of the different cases described in section 3, therefore providing critical information about the aqueous and environmental histories of Mars.

5. Conclusions

We have presented here geochemical models useful to understand future ground data on Li isotopic fractionation on the surface of Mars, obtained by landers and/or rovers. Our models can be used to describe the paths of Li isotopic fractionation, and therefore to characterize the extent of basalt weathering, the temperature at which the geochemical processes occurred, and the supersaturation and evaporation rates of the initial solutions in contact with basalt rocks on early Mars. Our results suggest that the analysis of δ^7Li trends in the Mars sedimentary record could be highly informative about the duration and intensity of pH fluctuations in the Martian paleoenvironments. Because such pH fluctuations were likely induced by changes in the CO_2 fugacity in the Martian atmosphere, the analysis of δ^7Li trends could also provide relevant information about the density and the temporal evolution of the atmosphere of Mars. This is an ongoing effort and additional scenarios are being developed and will be published in the future. Coupling the information from Li isotopes with Mg and maybe Fe and B isotopes could be of interest to further constrain the weathering environment of Martian alteration products [*Dauphas et al*., 2010; *Teng et al*., 2010]. The application of our models to the data obtained by future missions will contribute to deciphering the history of water and climate on Mars.

Acknowledgments
Data supporting our models and calculations are available as supporting information. The research leading to these results is a contribution from the Project "icyMARS", funded by the European Research Council, Starting Grant no 307496. This work was also partially supported by the European FEDER program and the Spanish Ministry of Science (MICINN) through the project CGL2011–30079. Comments by R. James and four anonymous reviewers helped us to clarify and strengthen our work.

References

Appelo, C. A. J., A. Vinsot, S. Mettler, and S. Wechner (2008), Obtaining the porewater composition of a clay rock by modeling the in- and out-diffusion of anions and cations from an in-situ experiment, *J. Contam. Hydrol.*, *101*, 67–76.

Bandfield, J. L., V. E. Hamilton, and P. R. Christensen (2000), A global view of Martian surface compositions from MGS-TES, *Science*, *287*, 1626–1630.

Beck, P., J. A. Barrat, M. Chaussidon, P. Gillet, and M. Bohn (2004), Li isotopic variations in single pyroxenes from the Northwest Africa 480 shergottite (NWA 480): A record of degassing of Martian magmas?, *Geochim. Cosmochim. Acta*, *68*(13), 2925–2933.
Bishop, J. L., et al. (2008), Phyllosilicate diversity and past aqueous activity revealed at Mawrth Vallis, Mars, *Science*, *321*(5890), 830–833.
Bishop, J. L., H. D. Makarewicz, W. P. Gates, N. K. Mckeown, and T. Hiroi (2010), Beidellites: Spectral properties and importance for Mars, *41st Lunar and Planetary Science Conference (2010)*, LPI. Abstract #2080, The Woodlands, Tex.
Bishop, J. L., W. P. Gates, H. D. Makarewicz, N. K. McKeown, and T. Hiroi (2011), Reflectance spectroscopy of beidellites and their importance for Mars, *Clays Clay Miner.*, *59*(4), 378–399.
Brant, C., L. A. Coogan, K. M. Gillis, W. E. Seyfried, N. J. Pester, and J. Spence (2012), Lithium and Li-isotopes in young altered upper oceanic crust from the East Pacific Rise, *Geochim. Cosmochim. Acta*, *96*, 272–293.
Burton, and Vigier (2011), in *Handbook of environmental isotope geochemistry*, edited by M. Baskaran, Springer Science & Business Media.
Carrol, D. (1959), Ion exchange in clays and other minerals, *Bull. Geol. Soc. Am.*, *70*, 749–780.
Chan, L. H., J. M. Edmond, G. Thompson, and K. Gillis (1992), Lithium isotopic composition of submarine basalts: Implications for the lithium cycle in the oceans, *Earth Planet. Sci. Lett.*, *108*, 151–160.
Chan, L. H., J. M. Gieskes, C. F. You, and J. M. Edmond (1994), Lithium isotope geochemistry of sediments and hydrothermal fluids of the Guaymas Basin, Gulf of California, *Geochim. Cosmochim. Acta*, *58*, 4443–4454.
Chan, L. H., J. C. Alt, and D. A. H. Teagle (2002), Lithium and lithium isotope profiles through the upper oceanic crust: A study of seawater-basalt exchange at ODP Sites 504B and 896A, *Earth Planet. Sci. Lett.*, *201*, 187–201.
Chan, L.-H., and F. A. Frey (2003), Lithium isotope geochemistry of the Hawaiian plume: Results from the Hawaii Scientific Drilling Project and Koolau Volcano, *Geochem. Geophys. Geosyst.*, *4*, 8707.
Chevrier, V., F. Poulet, and J.-P. Bibring (2007), Early geochemical environment of Mars as determined from thermodynamics of phyllosilicates, *Nature*, *448*(7149), 60–63.
Christensen, P. R., J. L. Bandfield, M. D. Smith, V. E. Hamilton, and R. N. Clark (2000), Identification of a basaltic component on the Martian surface from thermal emission spectrometer data, *J. Geophys. Res.*, *105*(E4), 9609–9621.
Christensen, P. R., et al. (2004), Initial results from the Mini-TES experiment in Gusev Crater from the Sprit Rover, *Science*, *305*, 837–842.
Christensen, P. R., et al. (2005), Evidence for magmatic evolution and diversity on Mars from infrared observations, *Nature*, *436*, 504–509.
Dauphas, N., F.-Z. Teng, and T. N. Arndt (2010), Magnesium and iron isotopes in 2.7 Ga Alexo komatiites: Mantle signatures, no evidence for Soret diffusion, and identification of diffusive transport in zoned olivine, *Geochim. Cosmochim. Acta*, *74*, 3274–3291.
Decarreau, A., N. Vigier, H. Pálková, S. Petit, P. Vieillard, and C. Fontaine (2012), Partitioning of lithium between smectite and solution: An experimental approach, *Geochim. Cosmochim. Acta*, *85*, 314–325.
Decitre, S., M. Buatier, and R. James (2004), Li and Li isotopic composition of hydrothermally altered sediments at Middle Valley, Juan De Fuca, *Chem. Geol.*, *211*(3–4), 363–373.
Ehlmann, B. L., G. Berger, N. Mangold, J. R. Michalski, D. C. Catling, S. W. Ruff, E. Chassefière, P. B. Niles, V. Chevrier, and F. Poulet (2013), Geochemical consequences of widespread clay mineral formation in Mars' ancient crust, *Space Sci. Rev.*, *174*(1–4), 329–364.
Fairén, A. G., D. Fernández-Remolar, J. M. Dohm, V. R. Baker, and R. Amils (2004), Inhibition of carbonate synthesis in acidic oceans on early Mars, *Nature*, *431*, 423–426.
Fairén, A. G., A. F. Davila, L. Gago-Duport, R. Amils, and C. P. McKay (2009), Stability against freezing of aqueous solutions on early Mars, *Nature*, *459*, 401–404.
Fairén, A. G., A. F. Davila, L. Gago-Duport, J. D. Haqq-Misra, C. Gil, C. P. McKay, and J. F. Kasting (2011), Cold glacial oceans would have inhibited phyllosilicate sedimentation on early Mars, *Nat. Geosci.*, *4*, 667–670.
Filiberto, J., E. Chin, J. Day, I. A. Franchi, R. C. Greenwood, J. Gross, S. C. Penniston-Dorland, S. P. Schwenzer, and A. H. Treiman (2012), Geochemistry of intermediate olivine-phyric shergottite Northwest Africa 6234, with similarities to basaltic shergottite Northwest Africa 480 and olivine-phyric shergottite Northwest Africa 2990, *Meteorit. Planet. Sci.*, *47*(8), 1256–1273.
Flesch, G. D., A. R. Anderson, and H. J. Svec (1973), A secondary isotopic standard for $^{6}Li/^{7}Li$ determinations, *Int. J. Mass Spectrom. Ion Phys.*, *12*, 265–272.
Gaines, G. L., Jr., and H. C. Thomas (1953), Adsorption studies on clay minerals II. A formulation of thermodynamics of exchange adsorption, *J. Chem. Phys.*, *21*, 714–718.
Gates, W. P., J. L. Bishop, H. D. Makarewicz, N. K. McKeown, and T. Hiroi (2010), Presence of beidellites on the Martian surface, in Extended Abstracts, *21st Australian Clay Minerals Conference*, pp. 19–22, Brisbane.
Gislason, S. R., and E. H. Oelkers (2003), Mechanism, rates, and consequences of basaltic glass dissolution: II. An experimental study of the dissolution rates of basaltic glass as a function of pH and temperature, *Geochim. Cosmochim. Acta*, *67*, 3817–3832.
Gislason, S. R., E. Oelkers, and A. Snorrason (2006), Role of river-suspended material in the global carbon cycle, *Geology*, *34*, 49–52.
Glynn, P. D., and E. J. Reardon (1990), Solid-solution aqueous-solution equilibria: Thermodynamic theory and representation, *Am. J. Sci.*, *290*, 164–201.
Gournis, D., A. Lappas, M. A. Karakassides, D. Többens, and A. Moukarika (2008), A neutron diffraction study of alkali cation migration in montmorillonites, *Phys. Chem. Min.*, *35*, 49-58.
Hathorne, E. C., and R. H. James (2006), Temporal record of lithium in seawater: A tracer for silicate weathering, *Earth Planet. Sci. Lett.*, *246*, 393–406.
Herd, C. D. K., A. H. Treiman, G. A. McKay, and C. K. Shearer (2004), The behavior of Li and B during planetary basalt crystallization, *Am. Mineral.*, *89*(5–6), 832–840.
Herd, C. D. K., A. H. Treiman, G. A. McKay, and C. K. Shearer (2005), Light lithophile elements in Martian basalts: Evaluating the evidence for magmatic water degassing, *Geochim. Cosmochim. Acta*, *69*(9), 2431–2440.
Hofmann, V. U., and R. Klemen (1950), Verlust der Austauschfahigkeit von Lithiumionen an Bentonit durch Erhitzung, *Z. Anorganiche Chem.*, *262*, 95–99.
Huh, Y., L. H. Chan, L. Zhang, and J. M. Edmond (1998), Lithium and its isotopes in major world rivers: Implications for weathering and the oceanic budget, *Geochim. Cosmochim. Acta*, *62*, 2039–2051.
Huh, Y., L. H. Chan, and O. A. Chadwick (2004), Behavior of lithium and its isotopes during weathering of Hawaiian basalt, *Geochem. Geophys. Geosyst.*, *5*, Q09002, doi:10.1029/2004GC000729.
Hurowitz, J. A., S. M. McLennan, D. H. Lindsley, and M. A. A. Schoonen (2005), Experimental epithermal alteration of synthetic Los Angeles meteorite: Implications for the origin of Martian soils and identification of hydrothermal sites on Mars, *J. Geophys. Res.*, *110*, E07002, doi: 10.1029/2004JE002391.
Hurowitz, J. A., W. W. Fischer, N. J. Tosca, and R. E. Milliken (2010), Origin of acidic surface waters and the evolution of atmospheric chemistry on early Mars, *Nat. Geosci.*, *3*(5), 323–326.

Jaynes, W. F., and J. M. Bigham (1987), Charge reduction, octahedral charge, and lithium retention in heated, Li-saturated smectites, *Clays Clay Miner.*, *35*(6), 440–448.
Jongsik, K., U. G. Nielsen, and C. P. Grey (2008), Local environments and lithium adsorption on the iron oxyhydroxides lepidocrocite (g-FeOOH) and goethite (a-FeOOH): A ^{2}H and ^{7}Li solid-state MAS NMR study, *J. Am. Chem. Soc.*, *130*, 1285–1295.
Kisakurek, B., R. H. James, and N. B. W. Harris (2005), Li and delta Li-7 in Himalayan rivers: Proxies for silicate weathering?, *Earth Planet. Sci. Lett.*, *237*, 387–401.
Lasaga, A. (1998), *Kinetic Theory of Earth Sciences, Princeton Ser. Geochem.*, Princeton Univ. Press, Princeton, N. J.
Le Deit, L., J. Flahaut, C. Quantin, E. Hauber, D. Mège, O. Bourgeois, J. Gurgurewicz, M. Massé, and R. Jaumann (2012), Extensive surface pedogenic alteration of the Martian Noachian crust suggested by plateau phyllosilicates around Valles Marineris, *J. Geophys. Res.*, *117*, E00J05, doi:10.1029/2011JE003983.
Liu, X. M., C. Wanner, R. L. Rudnick, and W. F. McDonough (2015), Processes controlling δ^{7}Li in rivers illuminated by study of streams and groundwaters draining basalts, *Earth Planet. Sci. Lett.*, *409*, 212–224.
Magna, T., U. Wiechert, and A. N. Halliday (2006), New constraints on the lithium isotope compositions of the Moon and terrestrial planets, *Earth Planet. Sci. Lett.*, *243*(3–4), 336–353.
McSween, H. Y., T. L. Grove, R. C. Lentz, J. C. Dann, A. H. Holzheid, L. R. Riciputi, and J. G. Ryan (2001), Geochemical evidence for magmatic water within Mars from pyroxenes in the Shergotty meteorite, *Nature*, *409*(6819), 487–490.
McSween, H. Y., et al. (2008), Mineralogy of volcanic rocks in Gusev crater, Mars: Reconciling Mössbauer, Alpha Particle X-Ray Spectrometer, and Miniature Thermal Emission Spectrometer spectra, *J. Geophys. Res.*, *113*, E06S04, doi:10.1029/2007JE002970.
McWorter, D. B., and D. K. Sunada (1977), *Ground-Water Hydrology and Hydraulics*, Water Resour. Publ., Fort Collins, Colo.
Merriam Jr, C. N., and H. C. Thomas (1956), Adsorption studies on clay minerals. VI. Alkali ions on attapulgite, *J. Chem. Phys.*, *24*(5), 993–995.
Meunier, A. (2005), *Clays*, Springer Science & Business Media.
Meyer, C. (2014), Mars Meteorite Compendium, JSC #27672, Revision C, Astromater. Res. and Explor. Sci., Johnson Space Cent., Houston, Tex.
Millot, R., N. Vigier, and J. Gaillardet (2010), Behaviour of lithium and its isotopes during weathering in the Mackenzie Basin, Canada, *Geochim. Cosmochim. Acta*, *74*, 3897–3912.
Misra, S., and P. N. Froelich (2012), Lithium isotope history of cenozoic seawater: Changes in silicate weathering and reverse weathering, *Science*, *335*(6070), 818–823.
Möhlmann, D., and K. Thomsen (2011), Properties of cryobrines on Mars, *Icarus*, *212*(1), 123–130.
Mustard, J. F., et al. (2008), Hydrated silicate minerals on Mars observed by the Mars Reconnaissance Orbiter CRISM instrument, *Nature*, *454*(7202), 305–309.
Odin, G. S., and P. D. Fullagar (1988), Geological significance of the glaucony facies, in *Green Marine Clays*, edited by G. S. Odin, pp. 295–332, Elsevier, Amsterdam.
Ollila, A. M., H. E. Newsom, B. Clark, N. Lanza, A. Cousin, R. C. Wiens, D. Vaniman, A. Rosen-Gooding, and MSL Science Team (2013), Lithium in the rocks and soils of Gale Crater, Mars, as observed by ChemCam, abstract presented at GSA Meeting, Geol. Soc. of Am., Denver, Colo.
Ollila, A. M., et al. (2014), Trace element geochemistry (Li, Ba, Sr, and Rb) using Curiosity's ChemCam: Early results for Gale Crater from Bradbury Landing Site to Rocknest, *J. Geophys. Res. Planets*, *119*, 1–31, doi:10.1002/2013JE004517.
Osthaus, B. B. (1954), Chemical determination of tetrahedral ions in nontronite and montmorillonite, *Clays Clay Miner.*, *2*(1), 404–417.
Palandri, J. L., and Y. K. Kharaka (2004), A compilation of rate parameters of water-mineral interaction kinetics for application to geochemical modeling, *U.S. Geol. Surv. Open File Rep.*, 2004-1068, pp. 1–64.
Parkhurst, D. L., and C. A. J. Appelo (1999), User's guide to PHREEQC (Version 2)—A computer program for speciation, batch-reaction, one-dimensional transport, and inverse geochemical calculations, *U.S. Geol. Surv. Water Resour. Invest. Rep.*, *99–4259*, pp. 1–64.
Pistiner, J. S., and G. M. Henderson (2003), Lithium-isotope fractionation during continental weathering processes, *Earth Planet. Sci. Lett.*, *214*, 327–339.
Pogge von Strandmann, P. A. E., K. W. Burton, R. H. James, P. van Calsteren, S. R. Gislason, and F. Mokadem (2006), Riverine behaviour of uranium and lithium isotopes in an actively glaciated basaltic terrain, *Earth Planet. Sci. Lett.*, *251*, 134–147.
Pogge von Strandmann, P. A. E., R. H. James, P. van Calsteren, S. R. Gíslason, and K. W. Burton (2008), Lithium, magnesium and uranium isotope behaviour in the estuarine environment of basaltic islands, *Earth Planet. Sci. Lett.*, *274*, 462–471.
Pogge von Strandmann, P. A. E., K. W. Burton, R. H. James, P. van Calsteren, and S. R. Gislason (2010), Assessing the role of climate on uranium and lithium isotope behaviour in rivers draining a basaltic terrain, *Chem. Geol.*, *27*, 227–239.
Pogge von Strandmann, P. A. E., H. C. Jenkyn, and R. G. Woodfine (2013), Lithium isotope evidence for enhanced weathering during Oceanic Anoxic Event 2, *Nat. Geosci.*, *6*, 668–672.
Russo, R. E., A. A. Bol'shakov, X. Mao, C. P. McKay, D. L. Perry, and O. Sorkhabi (2011), Laser ablation molecular isotopic spectrometry, *Spectrochim. Acta B*, *66*, 99–104.
Ryu, J.-S., N. Vigier, S.-W. Lee, K.-S. Lee, and O. A. Chadwick (2014), Variation of lithium isotope geochemistry during basalt weathering and secondary mineral transformations in Hawaii, *Geochim. Cosmochim. Acta*, *145*, 103–115.
Schmidt, M. E., et al. (2014), Geochemical diversity in first rocks examined by the Curiosity Rover in Gale Crater: Evidence for and significance of an alkali and volatile-rich igneous source, *J. Geophys. Res. Planets*, *119*, 64–81, doi:10.1002/2013JE004481.
Schultz, L. G. (1969), Lithium and potassium absorption, dehydroxylation temperature, and structural water content of aluminous smectites, *Clays Clay Miner.*, *17*, 115–149.
Seitz, H.-M., and A. B. Woodland (2000), The distribution of lithium in peridotitic and phroxenitic lithologies: An indicator of magmatic and metasomatic processes, *Chem. Geol.*, *166*, 47–64.
Seitz, H.-M., G. P. Brey, S. Weyer, S. Durali, U. Ott, C. Münker, and K. Mezger (2006), Lithium isotope compositions of Martian and Lunar reservoirs, *Earth Planet. Sci. Lett.*, *245*, 6–18.
Seitz, H.-M., G. P. Brey, J. Zipfel, U. Ott, S. Weyer, S. Durali, and S. Weinbruch (2007), Lithium isotope composition of ordinary and carbonaceous chondrites, and differentiated planetary bodies: Bulk solar system and solar reservoirs, *Earth Planet. Sci. Lett.*, *260*(3–4), 582–596.
Sposito, G. (1986), The polymer model of thermochemical clay mineral stability, *Clays Clay Miner.*, *34*(2), 198–203.
Steefel, C. I., S. Carroll, P. Zhao, and S. Roberts (2003), Cesium migration in Hanford sediment: A multisite cation exchange model based on laboratory transport experiments, *J. Contam. Hydrol.*, *67*, 219–246.
Stefansson, A., S. R. Gislason, and S. Arnorsson (2001), Dissolution of primary minerals in natural waters—II. Mineral saturation state, *Chem. Geol.*, *172*, 251–276.
Tang, Y.-J., H.-F. Zhang, and J.-F. Ying (2007), Review of lithium isotope system as a geochemical tracer, *Int. Geol. Rev.*, *49*, 374–388.

Taylor, S. R., and H. C. Urey (1938), Fractionation of the lithium and potassium isotopes by chemical exchange with zeolites, *J. Chem. Phys.*, *6*, 429–438.
Teng, F. Z., W. F. McDonough, R. L. Rudnick, and R. J. Walker (2006), Diffusion-driven extreme lithium isotopic fractionation in country rocks of the Tin Mountain pegmatite, *Earth Planet. Sci. Lett.*, *243*, 701–710.
Teng, F.-Z., R. L. Rudnick, W. F. McDonough, S. Gao, P. B. Tomascak, and Y. Liu (2008), Lithium isotopic composition and concentration of the deep continental crust, *Chem. Geol.*, *255*, 47–59.
Teng, F. Z., W.-Y. Li, R. L. Rudnick, and R. Gardner (2010), Contrasting lithium and magnesium isotope fractionation during continental weathering, *Earth Planet. Sci. Lett.*, *300*, 63–71.
Tertre, E., F. Hubert, S. Bruzac, M. Pacreau, E. Ferrage, and D. Prêt (2013), Ion-exchange reactions on clay minerals coupled with advection/dispersion processes. Application to Na^{+}/Ca^{2+} exchange on vermiculite: Reactive-transport modeling, batch and stirred flow-through reactor experiments, *Geochim. Cosmochim. Acta*, *112*, 1–19.
Tettenhorst, R. (1962), Cation migration in montmorillonites, *Am. Mineral.*, *47*, 769–773.
Theng, B. K. G., S. Hayashi, M. Soma, and H. Seyama (1997), Nuclear magnetic resonance and X-ray photoelectron spectroscopic investigation of lithium migration in montmorillonite, *Clays Clay Miner.*, *45*, 718–723.
Tomascak, P. B. (2004), Developments in the understanding and applications of lithium isotopes in the earth and planetary sciences, *Rev. Mineral. Geochem.*, *55*, 153–195.
Treiman, A. H., D. S. Musselwhite, C. D. K. Herd, and J. C. K. Shearer (2006), Light lithophile elements in pyroxenes of Northwest Africa (NWA) 817 and other Martian meteorites: Implications for water in Martian magmas, *Geochim. Cosmochim. Acta*, *70*(11), 2919–2934.
Verney-Carron, A., N. Vigier, and R. Millot (2011), Experimental determination of the role of diffusion on Li isotope fractionation during basaltic glass weathering, *Geochim. Cosmochim. Acta*, *75*, 3452–3468.
Vigier, N., A. Decarreau, R. Millot, J. Carignana, S. Petit, and C. France-Lanord (2008), Quantifying Li isotope fractionation during smectite formation and implications for the Li cycle, *Geochim. Cosmochim. Acta*, *72*, 780–792.
Vigier, N., S. R. Gislason, K. W. Burton, R. Millot, and F. Mokadem (2009), The relationship between riverine lithium isotope composition and silicate weathering rates in Iceland, *Earth Planet. Sci. Lett.*, *287*, 434–441.
Vorontsov, A. V., Yu. V. Novakovskaya, and N. F. Stepanov (2009), Comparative analysis of the state of lithium and sodium atoms in water clusters, *Russ. J. Phys. Chem. A*, *83*(7), 1134–1144.
Wiens, R. C., et al. (2012), The ChemCam instrument suite on the Mars Science Laboratory (MSL) rover: Body unit and combined system tests, *Space Sci. Rev.*, *170*(1–4), 167–227.
Williams, L., and R. Hervig (2005), Lithium and boron isotopes in illite/smectite: The importance of crystal size, *Geochim. Cosmochim. Acta*, *69*, 5705–5716.
Wimpenny, J., S. R. Gíslason, R. H. James, A. Gannoun, P. A. E. Pogge von Strandmann, and K. W. Burton (2010), The behaviour of Li and Mg isotopes during primary phase dissolution and secondary mineral formation in basalt, *Geochim. Cosmochim. Acta*, *74*, 5259–5279.
Wunder, B., F. Deschamps, A. Watenphul, S. Guillot, A. Meixner, R. L. Romer, and R. Wirth (2010), The effect of chrysotile nanotubes on the serpentine-fluid Li-isotopic fractionation, *Contrib. Mineral. Petrol.*, *159*, 781–790.
Zhang, L., L.-H. Chan, and M. Gieskes (1998), Lithium isotope geochemistry of pore waters from Ocean Drilling Program Sites 918 and 919, Irminger Basin, *Geochim. Cosmochim. Acta*, *62*, 2437–2450.
Zipfel, J., et al. (2011), Bounce rock-A shergottite-like basalt encountered at Meridiani Planum, Mars, *Meteorit. Planet. Sci.*, *46*, 1–20.
Zolotov, M. Y., and M. V. Mironenko (2007), Timing of acid weathering on Mars: A kinetic thermodynamic assessment, *J. Geophys. Res.*, *112*, E07006, doi:10.1029/2006JE002882.